SSW-008

Characterization of Coal Surfaces

by

Secondary Ion Mass Spectrometry

Final Report

by

N.S. McIntyre and W.J. Chauvin
Surface Science Western

and

R. R. Martin
Department of Chemistry

University of Western Ontario
London, Ontario N6A 3K7

Work on this project was conducted under the auspices of the Canada Centre for Mineral and Energy Technology, Energy Mines & Resources, Canada

DSS FILE NUMBER : 20SU.23440-1-9137

DSS CONTRACT SERIAL NUMBER : OSU82-00327

CANMET PROJECT NUMBER :

CANMET SCIENTIFIC AUTHORITY : Dr. J.A. McPhee

DATE: June 1983

This report should be cited as Contract Report No OSU-00327

72 pp

FEB 28 1984
MICROMEDIA

INDEX

Page

ABSTRACT 1

Statement of Work

Chapter 1 - Introduction

Chapter 2 - Experimental
(a) General Conditions
(b) Model Compounds
(c) Analysis of Coal Specimens

Chapter 3 - Vitrain

Chapter 4 - Fusinite

Chapter 5 - Exinite

Chapter 6 - Sub-bituminous Coal Studies

Chapter 7 - Oxidation of Vitrain

References

Tables 1 and 2

List of Figures

Abstract

Secondary Ion Mass Spectrometry (SIMS) has been used to analyze both the inorganic and organic constituents of coal. The high spatial resolution of the ion micorscope has been particularly important in obtaining characteristic spectra from this very heterogeneous material. Two distinct types of coal macerals: Vitrain , Fusinite and Exinite have been characterized as well as several examples of soft coal.

Negative secondary ion mass spectra are found to produce information more characteristic of the organic components of the coal, while positive secondary ions give a better determination of the inorganic elements. Negative ion images of carbon polymers appear particularly useful for providing enchanced structural detail of the coal surface, and certain chemical differences can also be recognized from the distribution of different carbon ion polymers. The spatial distributions have been imaged of a number of trace and minor concentrations of inorganic elements, including oxygen and hydrogen.

The maceral Vitrinite is characterized by a highly dispersed aluminosilicate inorganic phase with discrete particles of 5-15 μm diameter. Many other inorganic elements are detected within these particles in minor to trace concentrations. The organic phase between the particles is characterized by a high $C_2H_2^-/C^-$ value. There is evidence of chemical alteration of the organic phase in the immediate vicinity of the alumino silicate particles. The organic phase contains much of the titanium content of the coal, apparently in a well-dispersed form.

Fusinite was shown to have high concentrations of calcium and magnesium and fluorine dispersed evenly over large areas of the maceral (i.e. no discrete particles). The $C_2H_2^-/C^-$ ratio is noticeably lower than for vitrinite.

Exinite has been found to contain much lower concentrations of most inorganic elements than the surrounding matrix. In addition, a lower ratio of $C_2H_2^-/C^-$ compared to vitrinite allows exinite to be clearly imaged in the presence of the other maceral.

Some preliminary SIMS studies of the oxidation of vitrain are also reported.

Statement of Work

Ion Microscopy, a type of Secondary Ion Mass Spectrometry, is a highly sensitive analytical techniques capable of detecting virtually all chemical elements in microscopically small regions. It is considered a promising approach to characterizing the complex heterogeneous structures typical of coal.

The Cameca IMS-3F ion microprobe in the Surface Science Laboratory is to be used to evaluate the potential of coal microanalysis. The particular model of ion microprobe is considered the most technically advanced available with a capability of detecting many elements in the part per million range. Analytically difficult elements such as carbon and hydrogen are also detectable and their distribution determined to a resolution of 0.5 μm. Thus, both organic and inorganic phases can be characterized.

You are to perform the following tasks:

(1) Determination of appropriate instrumental conditions and sample preparation methods. This work will take approximately 4 days of instrument time.

(2) Detailed characterization of three distinct types of macerals using high resolution ion microscopy to determine fractional molecular weight values of the major organic ions. The fragmentation patterns produced by surface bombardment using O_2^+ will be compared with those obtained by fast atom bombardment(FAB) using a second mass spectrometer. This work will take approximately five (5) days of instrument time.

(3) Characterization of polished sections of fifteen (15) samples of Canadian coals selected by CANMET. This will be accomplished using:

(a) Mass spectra up to mass 500 of large regions of each coal;

(b) Ion imaging, giving the distribution of major ions produced on the surface;

(c) Line scans across the face of the coal sample, showing the distribution of major elements.

Approximately twelve (12) days of instrumental time will be required for this.

(4) Microscopic analysis of coal specimens to be analyzed by ion microprobe mass analysis both before and after SIMS analysis, for fifteen (15) samples.

CHAPTER I

Introduction

There are few geologic materials which exhibit as much complexity as coal. Most coals contain many separate inorganic and organic phases, which can only be distinguished at a microscopic level, if at all. Characterization and classification of coals has long been based on a microscopic analysis of the optical reflective properties and appearance of polished cross-sections, and this has led to the definition of certain coal macerals. Further understanding of the microscopic structure of coal has come from electron probe analysis of regions as small as 1 um, for chemical elements in the range from sodium to uranium.

This Report describes a new approach to the microcharacterization of coal, which makes use of Secondary Ion Mass Spectrometry (SIMS). This technique, which has recently begun to be used with other geologic materials (1), clearly has important advantages for understanding the inorganic and organic constituents of coal. SIMS involves the mass spectrometric analysis of ions which are removed from a surface by the action of a focussed primary ion beam. The secondary ions removed from the surface are characteristic of all elements present, and these may be identified mass spectrometrically by their mass numbers and isotope ratios. Very high detection sensitivites (ppb to ppm range) are often achieved with SIMS; moreover, this characteristic extends even to low atomic number elements which are difficult or impossible to detect by other surface spectrosocpies. Thus, a range of trace to major concentrations of inorganic elements in coal should be detectable in coals by SIMS, to a far greater extent than is possible with an electron microprobe(2).

In addition to inorganic analysis, SIMS has been able to provide characteristic mass spectra of many organic structures. Negative and positive secondary ion mass spectra have been obtained for structures such as graphite (3) and organic polymers (4-6). Such spectra often contain fragments of major structural groups and, in some cases, the molecular ion itself can be identified. Recently, the use of macroscopic SIMS for characterization of some organic constituents in coal itself has been reported (7). The related techniques, Fast Atom Bombardment (FAB) (8) and Plasma Desorption (7) have also been applied to the characterization of organic phases in coal. Several studies of laser microprobe (LAMMA) excitation of ions from coal surfaces has also been reported (9,10).

Secondary ion mass spectrometry also has a strong capability for analysis of microscopic regions. This capability is determined by the small diameter (2 μm) to which the primary ion beam can be focussed, or alternatively by the use of sophisticated ion optics to image the source of the secondary ions. No SIMS studies have yet been reported of coal microstructure, even at a modest (~100 μm) lateral resolution. Since many of the larger features identified in coal petrogrpahy are in this range, it is clearly advantageous to use SIMS with a lateral resolution of at least a few microns, in order to obtain unambiguous information from some of the regions.

In this report we describe the SIMS analysis of characteristic macerals which are prevalent in Canadian coals: vitrain , fusinite and exinite . Both organic and inorganic phases of each specimen were characterized, and this information was used in the identification of further coal specimens submitted by the Scientific Authority.

As prerequisite to such studies, the effect of the primary ion on model organic and coal surfaces has been investigated in an effort to determine optimal conditions for detection of both inorganic and organic constituents. From this, it is possible to determine which organic fragments are most affected by changes in chemical structure of the coal.

These studies of coal microstructure represent the first stage of a larger effort to use SIMS to determine mechanisms of coal surface oxidation. Since oxidation rates will likely be strongly affected by local compositional differences, the use of a highly sensitive microanalytical technique such as SIMS is of particular importance to this work. A preliminary examination of surface oxidation by SIMS is described in this report.

CHAPTER II

Experimental

(a) General Conditions

A Cameca IMS-3F ion microscope was used for all Secondary ion Mass Spectrometry studies. The principles (2) and use (12) of this instrument have been described previously. For most studies an O_2^+ primary ion beam of 200-800 na current and 7.5 keV net energy was used. The 50 µm diameter beam was rastered over a 250X250 µm area, thus giving a net current density in the range 30-120 $\mu A/cm^2$. The current readings originally made in the primary column, were corrected using measurements made with a Faraday cup on the sample stage itself. Both positive and negative secondary ion mass spectra were usually taken.

Coal specimens were prepared for analysis by polishing to a 1 µm finish with an alumina abrasive on a silk-covered polishing wheel, using water as the only lubricant. The use of hydrocarbons was scrupulously avoided, both in the optical microscopic characterization and in the polishing steps.

Ion bombardment of certain of the specimens caused significant charging of the surface. In these cases, the specimen surface was sputter coated with a layer of gold with a thickness of 50-200 Å. Most coals analyzed by SIMS caused no change in the high vacuum conditions of the specimen chamber, despite their realtively high vapour pressures. Containment of volatile components was clearly assisted by the gold surface coating used for charge dispersion. Certain of the soft coals, however, had vapor pressures which caused source instabilities. Such coals (P271 and P668)

were heated overnight at 100°C in a vacuum oven. Subsequent SIMS analysis showed no further instabilities, thus indicating that volatiles could be successfully removed from the surface region using this method.

Figure 1 shows bar graph mass spectra of both positive and negative secondary ions obtained from a graphite surface using a primary current density of 50 A/cm^2 . A series of carbon and carbon-hydrogen molecular ions can be detected, e.g. C^+, CH^+, CH_2^+, C_2, C_3^+, etc. In the negative secondary ion spectrum, the complement of organic ions is more intense and better defined, partly because of the lower contribution of inorganic species.

The effect of primary ion current on the relative concentrations of certain negative hydrocarbon ion fragments in the spectrum wasstudied, using the $^{12}C^-$ intensity as a standard.

In Figure 2 the change in the intensity ratio H^-/C^- is plotted as a function of O_2^+ primary beam current for both graphite and polystyrene. It can be seen that: (1) the ratio of H^-/C^- detected is quite different for the two materials analyzed; (2) the ratio of H^-/C^- for polystyrene changes markedly as function of beam current, the largest ratio being produced atvery low currents. The effect of using a different primary, Ar^+, in place of O_2^+ was also investigated for polystyrene and was found to produce a even higher H^-/C^- ratio.

The ratio $C_2H_2^-/C^-$ was also followed aschemical structure and beam current was changed. Figure 3 plots this ratio as a function of O_2^+ primary current density for both polystyrene and graphite.

In this case there is an even stronger difference in the ratio for polystyrene and graphite. The marked change in $C_2H_2^-/C^-$ ratio for polystyrene, as a function of current density, suggests that major changes in the mechanism of decomposition-recombination occur as beam density is increased. At the lowest current densities the SIMS spectrum for polystyrene was found to be similar to that reported by Briggs and Wooton (4) using static-SIMS conditions.

It is clear that from the point of view of obtaining relevant organic molecular ion information, the lowest current densities should be employed. For practical purposes, in this present study, current densities 100 times higher were used. Only under these conditions is it possible to detect many of the trace inorganic constituents in the coal matrix. Moreover, imaging of secondary ion distribution requires ion intensities considerably higher than those obtained at 0.5 nA beam current or lower.

The use of ion imaging is demonstrated in Figure 4 for a graphite surface. In this figure images of the $^{12}C^-$, H^-, C_2^- and C_2H^- distributions are shown across a 150 μm field. The $^{12}C^-$ image is almost featureless, while the C_2^- image evidently contains greater detail. It is possible that $^{12}C^-$ intensity is particularly flat because of the large contribution of small carbon impurities such as methane in the matrix. Thus, as higher molecular fragments are imaged more detail of the actual differences in chemical structure is revealed. The H^- image shows that certain areas of the graphite contain decidedly higher concentrations of hydrogen or hydrocarbons. A similar general distribution is seen in the C_2H^- image, but with enhanced resolution.

(c) Analysis of Coal Specimens

The principle aims of the analysis of the first samples supplied were twofold:
(a) To establish the optimum surface preparation required for SIMS analysis.
(b) To explore the capabilities of the instrument for the examination of such complex material. For this reason detailed petrographic analysis was not undertaken, rather, reliance was placed on the analysis supplied by the Scientific Authority (Table 1). It is clear that with such data, and without detailed optical microscopic examination directly related to the areas probed by the ion beam, some ambiguity will remain in the assignment of ion images to a specific maceral type. In view of this situation the first coal sample reported will be referred to as vitrain rather than vitrinite following the more general usage suggested by Neavel(11).

Subsequent microscopic examination of the coal showed a generally uniform surface, Figure 10, though semifusinite and fusinite inclusions are frequently in evidence. It is imperative to note that this retrospective examination was not greatly productive because the surface could not be correlated easily with the ion pits which had been altered during polishing to remove the gold used to improve the conductance of the samples.

(i) Mass Spectra

Typical log scale mass spectra of positive and negative ions for a vitrain specimen are shown in Figure 5. It is clear that one of the components of both spectra is a recurring series of peaks separated by 12 mass units, similar to, but not exactly like the spectra seen for graphite and polystyrene. A comparison of the graphite spectra, in Figure 1 with those of coal, is useful in determining differences due to the presence of inorganic constituents, the presence of organic functional groups and of other structural differences which result in entirely new fragmentation patterns.

The positive ion spectra of vitrain (Figure 5) can be better assessed by overlaying the pattern resulting from relatively pure graphite. Inorganic constituents such as Li, B, O, Na, Al, Si, S and Ca are clearly identifiable above the graphite background, from their known isotopic abundances. Above mass 40, the presence of inorganic molecular ions (SiO_n^+, CaO^+ etc.) makes it difficult to identify elements such as iron, without using high mass resolving power (2) or kinetic energy analysis (12). The presence of certain molecular ions, such as FeS^+ and its higher molecular weight combinations (FeS_2^+, $FeSO^+$, etc.) usually provides a clear identification of iron. In addition to identifiable inorganic atomic and molecular ions, there remain certain ions which cannot be correlated to a graphite-like spectrum. Particularly prominent are the peaks marked in Figure 1 m/e = 60, 61, 79 and 83 and those at higher mass (not shown), 113, 121 and 170. These peaks are believed to be due to specific organic structures, unrealted to the graphite skeleton used as a model.

A comparison of the negative ion spectra for graphite and the vitrain specimen shows that, aside from O, F, S, and Cl, there is a substantially lower contribution from other inorganic species. Thus, it is clearly easier to use the negative ion spectrum to characterize the organic components of the coal. The spectrum for graphite shows a recurring group of peaks every 24 mass units. A similar pattern is observed for vitrain , but the relative peak intensities within each group are substantially different than for graphite. For example, the ratio of m/e = 26/12 ($C_2H_2^-/C^-$) differs by over a factor of ten between the graphite and the vitrain spectra. This could result from a much greater contribution of hydrocarbon chains in the coal which cause an increase in the production of the ion $C_{2n}H_2^-$. Such differences were previously seen in the spectra of graphite and polystyrene. In addition, prominent peaks appear at certain mass numbers which are not accounted for as part of the skeleton carbon structure, just as in the positive ion spectrum. Thus, peaks at m/e = 42, 59, 76, 77, 79 are at least ten fold more intense than those for the graphite model. The relatively high primary beam energy and current used in these experiments appears to preserve few of the higher molecular weight fragments which might be expected from coal. Most of the earlier SIMS (5) and laser microprobe studies have also found that most prominent lines occur in the mass region below m/e = 100. Many more high molecular weight fragments are, however, observed in Plasma Desorption spectra of coal (7).

A reduction of the net accelerating voltage of 2keV resulted in a substantial increase in the organic fragments observed from the same area of the maceral. In Figure 6, prominent lines due to organic fragments can be identified at m/e = 42, 59, 95, 103, 119, 137, 179 and 197. Additional higher molecular weight peaks (not shown) are found at m/e = 213, 221 and 239. The peaks at

m/e = 239 and 197 and 221, 179, 137 and 95 are all separated by 42 mass units, while differences of 18 are frequently found between mass fragments, e.g. between 239 and 221 and 197 and 179. Thus, it seems possible that water (m/e = 18) elimination is a major route for the fragmentation of these molecules. The mass 42 fragment could be a carbonyl structures such as $H_2C\text{-}C{=}O$. In contrast, a previous Plasma Desorption study (7) of coal gave mass spectra whose major fragments were spaced by 44 mass units.

(ii) Line Scans

Microscopic features can be analyzed by either reducing the size of the primary ion beam to a few micrometers diameter, or reducing the size of the imaging field aperture. Changes in ion intensities across a surface can then be monitored by mechanically stepping the specimen stage past the beam. The effect of such a beam passage on a gold-coated coal surface is shown in the Scanning Electron Micrograph in Figure 7. The narrow band in the centre of the photograph defines the position traced by the primary ion beam. The broader band shows the area sputtered by a beam of primary neutrals which are approximately one percent of the intensity of the ion beam. Their flux, however, is sufficient to sputter away the gold surface layer.

A negative secondary ion line scan of the region traversed in Figure 7 is shown in Figure 8. Two separate traverses are shown for the ions H^-, C^-, C_2^-, C_6^- and $C_6H_2^-$ and the reproducibility is seen to be good. Any changes in reproducibility would arise from sputter-induced changes in composition during the traverse. The two dark featureless bands seen in Figure 7 are identified with reduced intensities of C_2^-, H^- and C_6^-. Such areas may be associated with a smaller density of complex hydrocarbons. Such changes in intensity are reflected more sharply in the higher molecular weight ions.

(d) Ion Microscopic Analysis - Using the ion imaging capability of the IMS-3F (11), an example of the distributions of a number of positive and negative ions is shown for a vitrain specimen. The distribution of $^{16}O^-$ was found to be particularly useful for identifying areas rich in inorganic oxides (see Figure 9). The oxygen is concentrated in aggregates 10-50 um in length, while the remaining areas have an oxygen ion intensity at least ten fold lower, as determined by a quantitative line scan across both regions. The oxide concentration could be at least partly identified with silicon (Figure 9 (b)) and aluminum (not shown) distributions.

Further chemical information on the region in Figure 9 was revealed by other ion images. The major distribution of OH^- (see Figure 9(c)) was found to follow approximately the same pattern as O^-, but the presence of strong point sources of m/e = 17 suggests that the hydroxyl ions are concentrated in much smaller pockets within the general oxide region. In addition, hydroxyl ion appears to originate, in lesser concentration, from within the low-oxygen areas shown in Figure 4(a). The ability to distinguish a chemical difference between oxygen and hydroxide distribution is important to future oxidation work. It is not clear however whether the OH^- ion results from water chemically or physically found in the coal or from actual hydroxyl groups. Localized pockets of fluoride (m/e = 19) are also detectable in this maceral (Figure 9(d)).

In Figure 9(e) and (f) the images of C^- and C_4^- distributions on the coal surface are compared. As in the graphite ion images, little detail of the coal surface structure can be determined from the C^- image, aside from the areas which are shown to be high in oxygen (and inorganic oxides) in Figure 9(a). By contrast,

in the carbon dimer, trimer and higher polymer images, an increasing amount of surface structure becomes evident. The detail in the C_3^- and C_4^- images is strongly reminiscent to transmission optical images of coal observed during petrographic examination. The changes in carbon polymer intensities may be a sensitive probe of carbon surface density.

CHAPTER III

Vitrain

(a) General Characteristics

One vitrain specimen from a sub-bituminous Eastern Canadian coal, submitted by the Scientific Authority, was subjected to extensive characterization of four separate areas by SIMS. The results of earlier petrographic and chemical analysis of the specimen are given in Table 1. An optical micrograph, of a random area of the polished surface, is shown in Figure 10. SIMS analysis of several representative areas is described below.

(b) Area 1

This particular area has already been described in detail in Chapter II, as an example of the use of ion microscopy on coals. The inorganic constituents are clearly collected into the distinctive "pebbled" oxygen-rich area, 10-25 μm in size, containing within them rather even distributions of silicon (Figure 9(b)) and aluminum. Within such areas, the intensities of carbon and its polymers are strongly reduced (Figure 9(e)) thus suggesting that the inorganic constituents have reached major concentrations. The hydroxyl (OH^-) distribution for Area 1 is particularly interesting for it is clearly not exclusively tied to O^- distribution. This suggests that areas rich in inorganic hydroxides or possibly water will give unique OH^- signals which are distinguishable from the O^- signals arising from inorganic oxides. Occasional small areas containing fluoride are detected, and these generally overlap with OH^- containing regions. Since F^- and OH^- frequently interchange in inorganic structures, the origin of the OH^- concentrations may, in fact, be inorganic hydroxides.

The carbon polymer images, C_3^-, C_4^-, etc. taken within Area 1 are unique in this present study. The intensity distributions (see, for example Figure 9(f)) suggest

the detection of structure which appears disarmingly close to that of plant cells.

(c) Area 2

This area, illustrated as a 400 μm field in Figure 11, has a much lower overall oxygen intensity. Moreover, the distribution of the oxygen is largely in particles 5 μm in diameter. The absence of many depleted zones in the carbon images suggests that most of the oxide detected is low in concentration and not heavily tied to inorganic constituents. Most of the oxygen regions detected are of considerably lower relative intensity than in Area 1. Both carbon images, C_2^- and C_4^- are generally featureless and this strongly suggested a very even carbon structure, containing few inorganics as oxides.

(d) Area 3

Area 3, like Area 1, has significant inorganic content, but in different distribution. Both positive and negative ion images of this region of the vitrain are shown in Figure 12 and it is interesting to compare the information obtained from ions of differing charge. Figure 12(a) shows a O^- image of a region containing a large area of inorganic oxide-rich material and a smaller organic-rich region. Images of $^7Li^+$ (Figure 12(b)) and $^{23}Na^+$, $^{27}Al^+$, and $^{28}Si^+$ (not shown) show a layered structure of inorganics, presumably resulting from sedimentation, and these agree reasonably well with the general oxygen distribution. Negative ion images appear much sharper than the complementary positive ion images. In contrast to the above inorganic ion distribution, the major amount of titanium present, detected as $^{48}Ti^+$, is rather evenly distributed throughout the organic-rich region. (See Figure 12(c)). This result suggests the possibility that titanium is bonded as an organic complex, rather than as a mineral. The form of titanium in coal is of interest since titanium poisons

catalysts during coal liquifaction (12). Images for both H^- and H^+ are shown in Figure 12 (d) and (h). It is clear that the H^+ is associated almost entirely with inorganic oxide regions and thus must arise from hydrate decomposition. By contrast, the negative H^- ion appears to be distributed across the same organic-rich regions as C^-; this suggests its association mainly with organic groups.

The image of C^- (Figure 12(e)) ions from the surface reflects the increased quantity of carbon in the organic-rich regions of the specimens. As in the previous specimen greater structural detail of the surface is obtained from the C_2^- image. Comparison of the C_2^- (m/e = 24) and $C_2H_2^-$ (m/e = 26) images (Figures 12(f) and (g)) suggests further differences, perhaps in the chemical nature of the carbon in different locations. The intensity of $C_2H_2^-$ has been shown already to be particularly susceptible to chemical effects. In Figure 12 (g), the $C_2H_2^-$ intensity in the immediate vicinity of the oxide particles, appears to be distinctly lower.

Further information on the relationship of $C_2H_2^-$ in oxidized regions can be obtained from line intensity scans through regions containing both high and low concentrations of oxygen. Line scans shown in Figure 13 (a) and (b) were taken through portions of Area 3, so as to include a region high in oxygen, as well as one low in oxygen. This scan of C^-, O^-, OH^-, C_2^- and $C_2H_2^-$ in fact allows a quantitative measure of the intensity change in O^- which produces the contrast seen in Figure 12(a). In Figure 13(a) a change in oxygen intensity of almost 15 times is seen between the two extremes. Within the low oxygen area ($O^-/C^- = 0.8$), a C_2H_2/C^- ratio of 12 is obtained, while in the high oxygen

area the same ratio has fallen to 7. Figure 13(b) explores this relationship in further detail. A line scan through another area containing high oxygen areas shows that the $C_2H_2^-/C^-$ ratio is not a direct function of the O^-/C^- ratio, but rather it decreases to its lowest level ($C_2H_2^-/C^- = 2$) in the midst of the oxygen particles. This may be seen in better detail in Figure 12(g) where the $C_2H_2^-$ image is darker in the vicinity of the oxide particles. This suggests that the presence of such oxides may be affecting the chemical composition of the organic phases in their vicinity.

The C_2^-/C^- ratios in the line scans do not change significantly. Changes in C^- intensity due to topographical or other changes appear to cause an exaggerated response in the C_2^- intensity. This is the same as the enhanced detail seen in the carbon polymer images.

(e) Area 4

Figure 14 shows 150 μm field images of another vitrain area containing significant quantities of inorganic ions. However, the distribution and composition of these is somewhat different from Areas 1 or 3. Figure 14(d) shows that oxygen is distributed in particles 5 μm thick and 1-20 μm in length. Other images (not shown) indicate that sodium, aluminum silicon and lithium are evenly distributed in the oxide-rich area. This is typical of the distribution seen in Area 3 which was ascribed to sedimentary origins. The C^- image suggests a relatively even distribution of carbon, while the C^+ image suggests carbon distribution similar to that seen for oxygen.

It is however possible that the positive C^+ intensities from these particles results from the presence of inorganic carbon, such as carbonates. This situation would thus be analogous to H^+ arising largely from inorganic hydrates and H^- resulting from organically bonded hydrogen.

A summary of typical negative ion intensity ratios for vitrinite and other macerals and coals analyzed is provided in Table 2. It should be emphasized that the Table is only intended to judge relative trends and not as a key for identifying a specific maceral. That particular task requires ion image and mass spectral analysis.

Mass spectra of the organic areas away from the particles showed that a $C_2H_2^-/C^-$ ratio as high as 12 was obtained. This differs considerably from the ratio for graphite and is higher than typical ratios found in other macerals (see below).

(f) Summary

Vitrinite contains many areas of densely packed inorganic oxides 5-30 um in diameter. These oxides contain lithium, sodium, silicon, aluminum, calcium, iron and barium distributed fairly evenly. The concentration of inorganic elements is of a high enough order to suppress the carbon signal by up to a factor of ten. It is suggested that carbonate is found within the inorganic phase in Area 4. Unfortunately, no observations of sulphur distribution were made because of a partial interference between O_2^- and S^- at mass 32.

CHAPTER 4

Fusinite

(a) General Characteristics

Two different specimens, identified petrographically as fusinite, were analyzed by SIMS. One of these, fusinite A, was a microscopic region, 70 X 300 μm in size, identified by Scientific Authority. The coal maceral(s) surrounding the fusinite were not identified. A Scanning electron micrograph of the fusinite is shown in Figure 15 (a). A second, much larger, specimen (usinite B) was also studied, and its micrograph is shown in Figure 15 (b).

(b) Fusinite A.

The area within the fusinite A maceral can be most clearly seen in the H^- image of the region in Figure 16(a). The organic hydrogen distribution is fairly even, in contrast to that in the surrounding matrix. Toward the centre of the maceral a slightly darker region is discerned which was found to produce elevated intensities of C^-, O^- and F^-. The high fluorine content of this area, about half the size of the whole maceral, can be seen from the line scan, in Figure 17, taken across the maceral. The fluorine concentration within this particular area is seen to be about 2 orders of magnitude above that in the Vitrinite (see Table 2). The $C_2H_2^-/C^-$ ratio within the maceral region is substantially lower than that found in an area of vitrain which had a low mineral content (see Table 2).

Figure 18 shows the positive ion images of several elements within fusinite A. The low H^+ concentration implies a lack of hydrated species and this is in accord

with the virtual absence of inorganic clay minerals such as aluminum sodium and potassium. Throughout most of the maceral, a general distribution of only magnesium and calcium is seen. Barium was evenly distributed over about one quarter of the maceral. If these elements are associated with particles within the maceral, then such particles would be less than 1 micrometer in diameter. It is also possible, that the magnesium and calcium have a biological origin, with a resultant distribution which could be relatively even.

(c) Fusinite B

A negative ion mass spectrum of a typical 250 micrometer square of this maceral is shown in Figure 19. Comparing this spectrum to that of a vitrain (see Figure 5), a much higher contribution to masses 72, 80, 88, 96 and 104 is seen for fusinite. These form a recurring pattern involving loss of 12 and 8 mass units. This suggests that a larger proportion of ions are left as hydrocarbons, compared to vitrain.

The distributions of $^{12}C^-$, $^{12}C^+$, $^{24}Mg^+$, $^{40}Ca^+$, $^{19}F^-$, $^{23}Na^+$, $^{27}Al^+$ and $^{28}Si^+$ are shown in Figure 20. The distributions of C^- and C^+ are, in general, quite similar, thus suggesting that carbonate is not a major contributor. As in fusinite A, significant intensity of F^- and Mg^+ were found, and, of greater importance, the distribution of these elements was rather even through the matrix. Calcium also is widely distributed although, as before, not as thoroughly as magnesium. Sodium and potassium (not shown) are present in high concentrations in a number of particles 10-15 μm in size. Their concentrations are high enough to suppress the intensity of carbon in those regions. These particular regions may be pores in the charred material, resulting from cell lumina, into which certain elements have been deposited by evaporation. The

distribution of aluminum and titanium (not shown) is significantly different from that of sodium while that of silicon is very diffuse.

(d) Summary

The major distinguishing characteristic of fusinite is the presence of an even distribution of magnesium and fairly even distribution of fluorine and calcium. Unlike the vitrain , most elements are <u>not</u> found grouped together as clay minerals, but rather they exhibit several different patterns of distribution. There appear to be some definite differences in the organic mass spectra of non-oxide vitrain and usinite and the $C_2H_2^-/C^-$ ratios reflect this.

CHAPTER 5

Exinite

Results and Discussion:

(a) General Characteristics

Two separate exinite macerals were identified petrographically by the Scientific Authority. Of these two the exinite A had the elongated and frilled shape of typical cutinite, while the second, exinite B, had the lens-like shape of sporinite. Although the identification of these sub-classifications could not be absolutely certain, these terms will be used in describing the two macerals. An optical micrograph of the cutinite within a vitrain matrix, is shown in Figure 21.

(b) Exinite A

Negative ion images of C^- and C_2^- (see Figure 22) no difference in intensity between the identified maceral and the surrounding matrix. The $C_2H_2^-$ image however, shows significant contrast between the exinite maceral and the surrounding vitrain. Thus the $C_2H_2^-/C^-$ ratio is clearly lower in exinite than in vitrain (see Table 2). The organic content of the Exinite is clearly different from that of the surrounding maceral.

All positive ion images show an almost complete lack of inorganic content in the exinite. The $^{24}Mg^+$ image in Figure 22 is illustrative of this, but similar patterns were obtained for sodium, fluorine, lithium, aluminum, silicon, potassium, titanium and iron. The distribution of these elements within particles in the vitrain is entirely similar to what was seen in the previously analyzed vitrain specimen.

(c) Exinite B

The sporinite (exinite B) was imaged in such a way that the maceral intruded into the imaged field at apoint between 1 and 3 o'clock in the image (see Figure 23). The positive ion images agreed with those taken previously for exinite A, in that the maceral contains particularly low concentrations of sodium, potassium, magnesium, aluminum and lithium, in comparison with the surrounding matrix (not identified). Minor particles containing calcium and iron are noted within the maceral but the overall concentration is much lower than in the surrounding matrix.

The negative ion images for sporinite had contrasts similar to those seen for cutinite, but not as distinct. No difference between the exinite and the surrounding area was detected in the C_2^- image, while for $C_2H_2^-$, the exinitic region was a darker contrast. This ion image information was confirmed by the mass spectra taken of both the exinitic and the surrounding regions. For the exinite, a $\frac{C_2H_2^-}{C^-}$ intensity ratio of 6 was measured, while for the area around the exinite, an intensity ratio of 9 was observed. No difference in the oxygen content is observed between exinite B and the surrounding matrix.

(b) Summary

Exinite is characterized by the much lower concentration of most inorganic consitituents, such as sodium, potassium, aluminum, magnesium, calcium, fluorine and titanium. In addition, the maceral has a lower $C_2H_2^-/C^-$ ratio than vitrain but probably about the same as fusinite.

CHAPTER 6

Analysis of Selected Coals

(a) Introduction

Several specimens of coal were submitted by the Scientific Authority for SIMS analysis using similar approaches to those used on the pre-characterized macerals. Each specimen was photographed through an optical microscope and typical areas are shown in Figure 24. All of these specimens were soft coals, containing a relatively large component of volatile material. It was thus necessary to heat each sample to 90°C overnight in a vacuum oven. Even with such precautions, the amount of outgassing was greater than with previously analyzed specimens, and this, at times, caused degradation in the quality of the ion images.

(b) P-251

Ion images of Ca^+, Al^+, O^- and C^- are shown in Figure 25 for the only area successfully imaged in this high volatiles coal.

A very large and relatively even concentration of calcium was found. The level of calcium, as well as fluorine and oxygen (see Table 2) in this coal was, in fact, so high that carbon ion intensities were substantially reduced, compared to previous coal analyses. The sulphur content was about 100 times higher than in the macerals studied. Concentrations of inorganics such as silicon and aluminum were much lower than calcium and both distributions differed substantially.

(c) P-251

Area 1 - Figure 26 shows intense ion images for C^+, Al^+, Si^+ and Sr^+. The silicon and aluminum (and magnesium) are distributed in a pattern strongly reminiscent of a sedimentation process, just as was observed previously for a vitrain specimen. Stontium and barium ionsof medium intensity are distributed in a pattern of 5-10 μm particles, different from the aluminosilicate distribution.

Area 2 - This area is markedly different in composition from Area 1 and has a particularly complex mineral structure. The major inorganic constituents are calcium, aluminum and barium, and all three are distributed very similarly with about half of the 150 μm field of observation covered evenly by these elements (see Figure 27). Silicon is oriented in a similar distribution, but is of lower overall intensity. Boron was detected and imaged in coal for the first time within this area. Boron appears to be largely associated with sodium and potassium, as determined by the overlap of distributions. The presence of these elements together suggests that this is a coal of marine origin. The composition within this area does not match that of any maceral studied to date.

(d) P-668

The one area imaged on this specimen contained very high, evenly distributed, concentrations of oxygen, fluorine, calcium. sodium and aluminum (see Table 2 and Fig. 28). Some very faint bands are detected in the coal, 10-20 μm in width, which

have a higher $C_2H_2^-/C^-$ ratio and slightly lower concentrations of elements, such as aluminum and sodium. On the basis of previous limited experience with other macerals, it is not possible to relate this region to any maceral previously examined. The high $C_2H_2^-/C^-$ ratio would suggest a vitrain area, but the image distributions show little evidence of sedimentation of minerals. The banding is not due to an exinitic region since no change in inorganic content is noted.

Summary - some of these highly oxidized sub-bituminous coals can, in part, be related to previously analyzed macerals.

CHAPTER 7

Oxidation of Vitrain

To assess the possibility for detecting alterations in the surface composition of the maceral during oxidation, a portion of the previously analyzed specimen of vitrain was subjected to oxidation. Conditions used were not untypical of those experienced by coal during storage.

The specimen was heated in a drying oven at 110°C for a period of 48 hours. Area 3 of the vitrain specimen was chosen for analysis after it had been previously examined by SIMS. A depth profile, shown in Figure 29 measured the relative concentrations of oxygen and several carbon species as a function of depth into the surface. The high O^- signal at the surface decreased with depth to an equilibrium value at an estimated depth of 400 nm. Similar profiles on unoxidized surfaces of the vitrain showed no concentration gradiant in oxygen.

One of the regions of the maceral which underwent oxidation contained the feature shown in Figure 12. New ion images were obtained of this region, working rapidly to remain within the oxidized surface thickness. Images of Li^+ and O^- are shown in Figure 30(a) and (b). There is considerable change in the O^- distribution compared with that in Figure 12(a). Definition of the oxygen-rich agglomerate is less clear, since it appears that increase in O^- intensity has been particularly noticeable in the region between the inorganic rich particles. The Li^+ image, is certainly much less altered in definition, thus showing that the haziness of the O^- image is not due to an alteration in the general optical quality of the coal surface.

The observation of altered oxygen concentration suggests that there may be some preferential oxidation in the immediate vicinity of the inorganic particles.

Summary - Both bulk and microscopic oxidation effects on the surface have been detected for relatively mild oxidation conditions of vitrain.

CHAPTER 8

Conclusions

This work represents the first attempt to relate elemental and chemical composition to microstructure within small coal macerals. It has been readily possible to obtain spatial distributions of many chemical elements to a resolution of 1 um. Detection limits vary with elemental sensitivity but imaging of most elemental distributions at the 0.1% level or better is possible in this matrix. This is well beyond the capabilities of other microanalytical techniques and as such has permitted a more detailed analysis of these distributions than in other reported work. Our effort has been directed toward exploring the differences in elemental distribution within several well defined coal macerals. The work, however, has not been undertaken in the belief that SIMS would provide a stand-alone method of identififying maceral types, but rather to learn if specific elemental and molecular distributions are unique to individual macerals and if such elemental analysis would provide evidence of the organic composition of such coals.

It has been relatively straightforward to prepare most coal specimens for SIMS analysis. It is necessary to avoid any hydrocarbons during specimen polishing, to reduce volaitles in soft coals by pre-heating and to use a conducting surface layer to reduce surface charging effects.

SIMS studies of model organic compounds, have contributed to our understanding of processes taking place during coal analysis.

Investigations of polystyrene and graphite have shown that both individual ion

yields and the ratios of ion yields are strongly dependent on primary beam current. This has allowed establishment of optimum conditions for analysis for specific ions under each of the modes of operation available in SIMS.

Each mode of SIMS analysis yields information of different value. The highest information density is obtained from ion images. These give distribution patterns of many elements which may be readily correleated. The intensity information, however, is not quantitative and supporting data must be obtained from elemental line scans. The detection of large organic molecules or fragments in mass spectra of the coal has clearly not been as useful. This is due, in part, to the relatively high ion fluxes used for detection of inorganic constituents. Under such conditions most high molecular weight fragments have decomposed. Subsequent analyses of organic constituents of certain macerals will be carried out using intensities 100-300 times lower than those used at this phase of the work. Under such near-static SIMS conditions, larger quantities of higher molecular weight specimens will result, and perhaps even be imaged. However, location of the exact area analyzed and its constituents will first have to be defined at conditions comparable to those in this work.

The organic structure of coal appears to be most effectively detected using negative secondary ions. Specifically ratios such as $\frac{C_2H_2^-}{C^-}$ promise to be a useful indication of changes in the organic strucutre. Eventually, it may be possibe to relate the numerical value of this ratio to some characteristic of the coal, such as its rank.

Studies of the oxygen content of coal have been undertaken and the relative concentration of this element throughout individual samples has been examined using line scans and imaging techniques. Similar information obtain for OH^-, H^+, H^-, C^+ and C^-, when correlated with these results is expected to indicate the distribution of functional groups in the organic molecular structure of the coal.

With the exception of Chapter 7, little has been said about coal surface properties; most of the effort has been directed toward the characterization of organic and inorganic micorstructures. The complexity of the oxidation process in a coal matrix requires an imaging technique capable of measurement in all three dimensions. One vitrain sample was subjected to mild air oxidation and the resulting changes in the surface oxygen were successfully imaged. The penetration of this oxygen into the bulk material was also studied using depth profiling. These procedures have suggested that SIMS may be used to carry out quite detailed analyses of the oxidation process in coal.

The distribution and chemical habit of inorganic elements have been imaged and analyzed. Common clay minerals can be readily identified and their mode of deposition in the coal may be inferred from this information. Evidence of layering of inorganics from sedimentation, and evaporative deposition in pores has been shown. The inorganic elements imaged in other coals, clearly results from the biological matrix itself. There is evidence that organometallic compounds may also be detected in coal. The identification of titanium with regions of the coal clearly organic in nature suggests that other metal organic structures can be identified.

There is little doubt that SIMS, in its imaging mode will be of value to future coal petrographic studies.

References

(1) Tingey, G.L., Lytle, J.M., Baere, D.R., Thomas, M.T.., Pacific Northwest Laboratory Report, PNL-350, 1 (1980)

(2) SIMS - btter for inorganics than electron microprobe. Gourgout, J-M., in Secondary Ion Mass Spectrometry SIMS-II, Springer-Verlag, New York, pp. 286, (1979)

(3) Whittaker, A.G. Carbon, 17, 21 (1979)

(4) Briggs, D. and Wootton, A.B., Surface and Interfacial Analysis 4, 109 (1982)

(5) Lampana, J.E., DeCorpo, J.J. and Colton, R.J. Appl. Surf. Sc. 8, 337, (1981)

(6) Winogard, N. and Karwacki, E.J., Anal. Chem., 55, 790 (1983)

(7) Lytle, J.M. Tingey, G.L., and McFarlan, Anal. Chem., 54, 1881 (1982)

(8) Taylor, L.C.E., Ind. Res./Dev., 23, 124 (1981)

(9) Joy, W.K., Ladner, W.R. and Pritchard, E. Fuel, 49, 26 (1970)

(10) Vanderborgh, N.E. and Roalnd Jones C.E., Anal. Chem. 55, 527, 1983

(11) Neavel, R.C. in Chemistry of Coal Utilization, vol. 2, John Wiley and Sons, pp. 98 (1981)

(12) Stodzian, G., in NBSPublication 427, National Bureau of Standards, Gaithersburg, MD 33 (1975)

Table 1

PETROGRAPHIC & CHEMICAL CHARACTERIZATION OF VITRINITIC COAL USED IN STUDY

Petrographic Analysis:	Vitrinite	76%
	Exinite	3%
	Micrinite	5%
	Semi-fusinite	8%
	Fusinite	8%
Proximate Analysis:	Moisture	0.8%
	Ash	2.4%
	Volatile Matter	34.3%
	Fixed Carbon	62.6%
Ultimate Analysis:	Carbon	84.3%
	Hydrogen	5.3%
	Sulphur	0.7%
	Nitrogen	2.1%
	Ash	2.4%
	Oxygen(by difference	4.2%

TABLE 2

ION INTENSITY RATIOS FOR SPECIFIC COAL MACERALS AND OTHER SPECIMENS ANALYZED

Specimen	Ion Ratio			
	$C_2H_2^-/C^-$	O^-/C^-	F^-/C^-	S^-/C^-
Vitrain - low oxygen region	12	0.5	<.1	<0.1
Vitrain - oxide-rich region	2	6	<.1	<0.1
Fusinite (F3)	1.2-4	1-2	4	0.05
Exinite	6-10	0.2-0.8	1-1.5	0.01
P-568	3	10	4	1
P-567	-	-	-	-
P-668 (range)	1.5	10	9	0.2
	11	2.5	2	0.2

LIST OF FIGURES

1. Bar graph mass spectra of graphite showing both positive and negative secondary ions

2. Ratio of H^-/C^- vs logarithim of primary ion beam current for graphite and polystyrene

3. Ratio of $C_2H_2^-/C^-$ vs logarithim of primary ion beam current for graphite and polystyrene

4. Negative ion images of a graphite surface showing C^-, H^-, C_2^- and C_2H^-

5. Bar graph mass spectra of vitrain showing positive and negative secondary ions

6. Negative ion bar graph mass spectrum of vitrain using low energy primary ions

7. SEM image of SIMS line scan area

8. Line scans of coal surface showing reproducibility of this method

9. Ion images of one area of vitrain showing O^-, Si^-, OH^-, F^-, C^- and C_4^-

10. Optical micrograph of a polished section of a vitrain specimen

11. Ion images of a second area of vitrain showing C_2^-, C_4^-, O^- and OH^-

12. Ion images of a third area of vitrain showing O^-, Li^+, Ti^+, H^+, C^-, C_2^-, $C_2H_2^-$ and H^-

13(a),(b). Line scans across vitrain macerals of varying oxygen content

14. Ion image of a fourth area of vitrain showing C^-, C^+, C_2^- and O^-

15(a),(b). Scanning electron micrograpahs of fusinite macerals after analysis by SIMS

16. Negative secondary ion images of a fusinite maceral showing H^-, C^-, F^- and O^-

17. Line scan through a fusinite maceral

18. Positive ion images of a fusinite maceral showing H^+, Al^+, Ca^+ and Mg^+

19. Bar graph mass spectrum of fusinite, negative secondary ions

20. Ion images of a fusinite maceral showing C^-, C^+, Mg^+, Ca^+, F^-, Na^+, Al^+ and Si^+

21. Optical micorgraph of exinite within a vitrain matrix

22. Ion images of exinite "A" showing C_2^-, $C_2H_2^-$ and Mg^+

23. Ion images of exinite "B" showing O^-, C_2^-, $C_2H_2^-$, Na^+, Mg^+ and Fe^+

24. Optical micrographs of typical areas of specimens 568, 587 and 668

25. Ion images of coal P-568 showing Ca+, Al^+, O^- and C^-

26. Ion images of first area coal P-587 showing C^+, Al^+, Si^+ and Sr^+

27. Ion images of second area of coal P-587 showing Ca^+, Al^+, Ba^+, Si^+, Na^+, and K^+

28. Ion images of coal P-668 showing O^-, F^-, Ca^+, Al^+, C^- and $C_2H_2^-$

29. Depth profile of oxygen concentration in mildly oxidized vitrain

30. Ion images of oxygen-induced changes of the microstructure of a vitrain surface

Figure 1 - Secondary Ion Mass Spectrum of a Graphite Surface

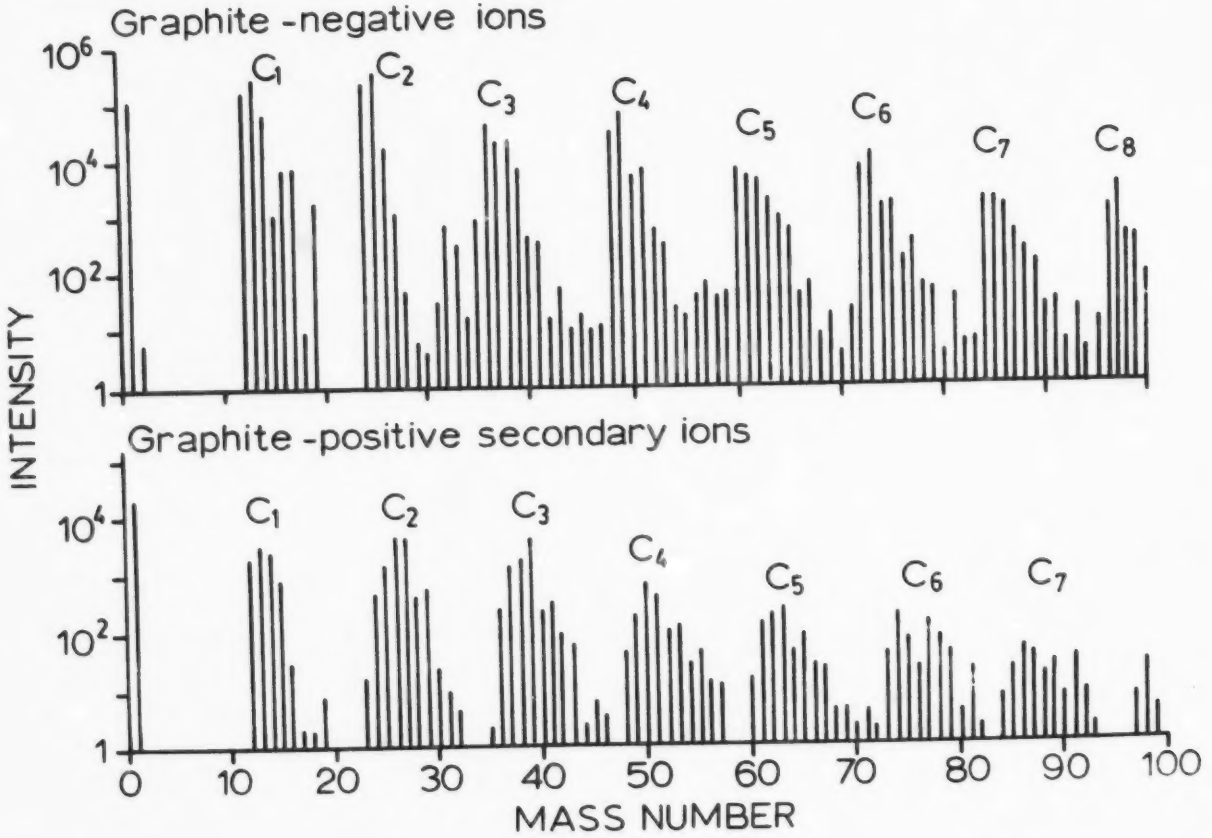

Figure 2 - Effect of Primary Ion Current Density on H^-/C^- Intensity Ratios for Two Organic Model Compounds

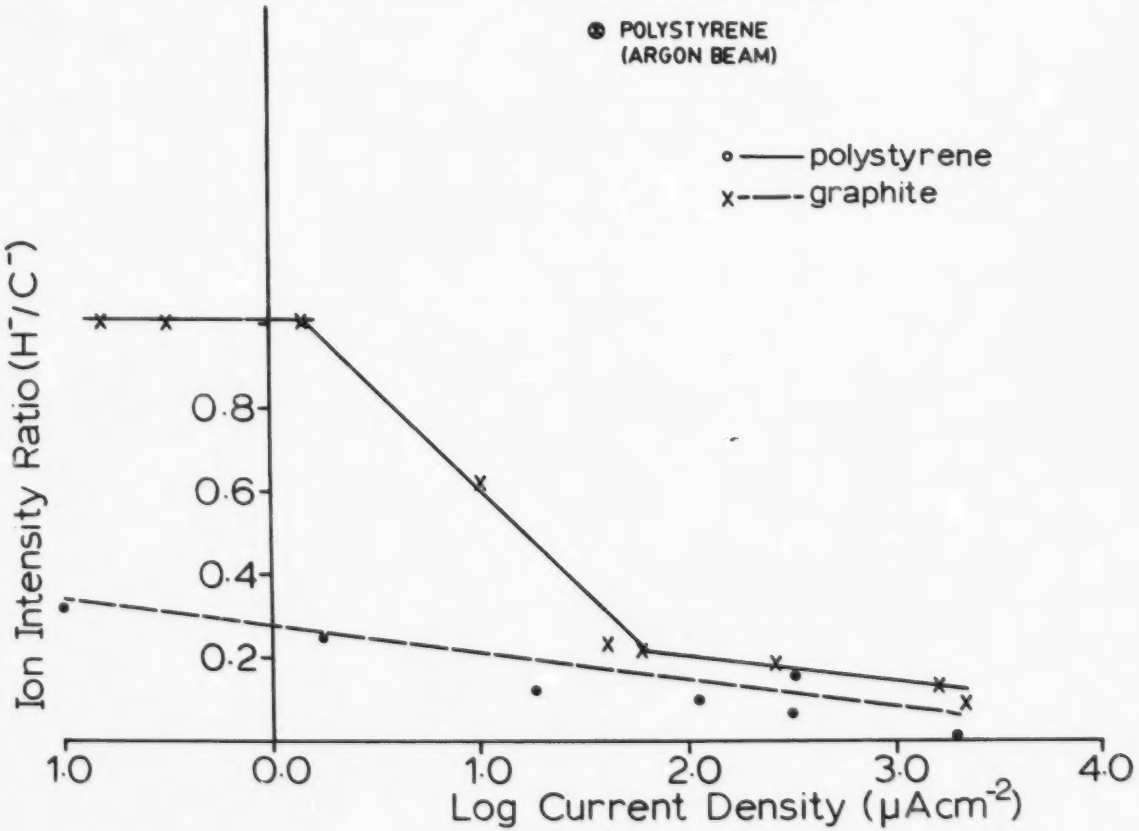

Figure 3 - Effect of Primary Ion Current Density on $C_2H_2^-/C^-$ Ratio for Two Organic Model Compounds

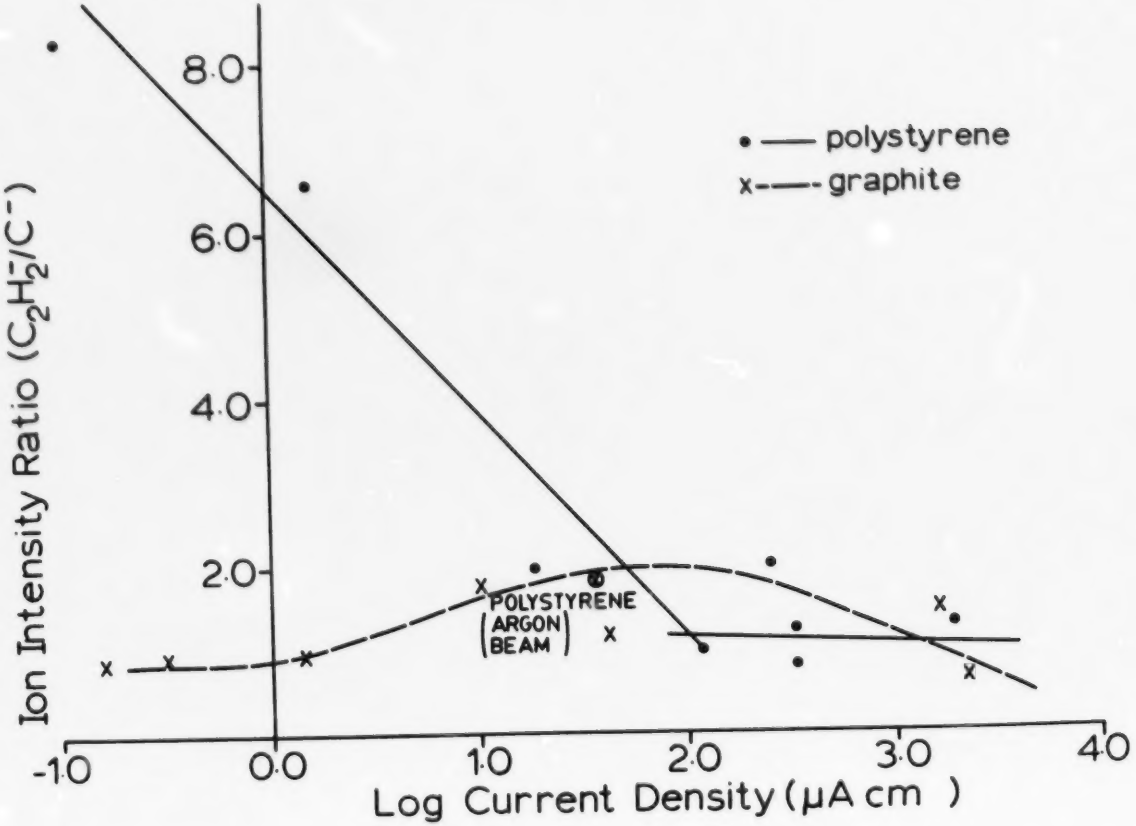

Figure 4 - Negative Ion Images of a Graphite Surface

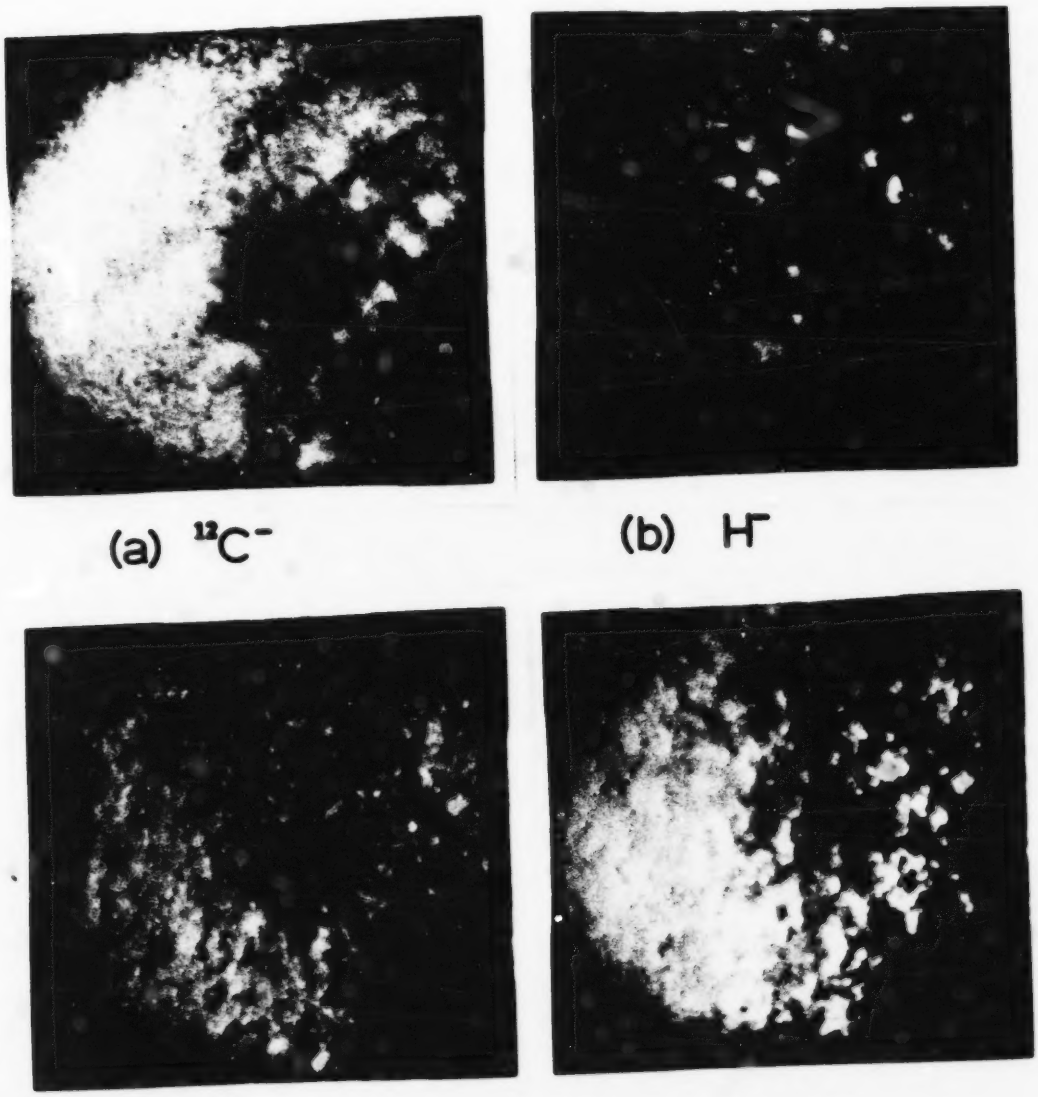

(a) $^{12}C^-$ (b) H^-

(c) C_2^- (d) C_2H^-

Figure 5

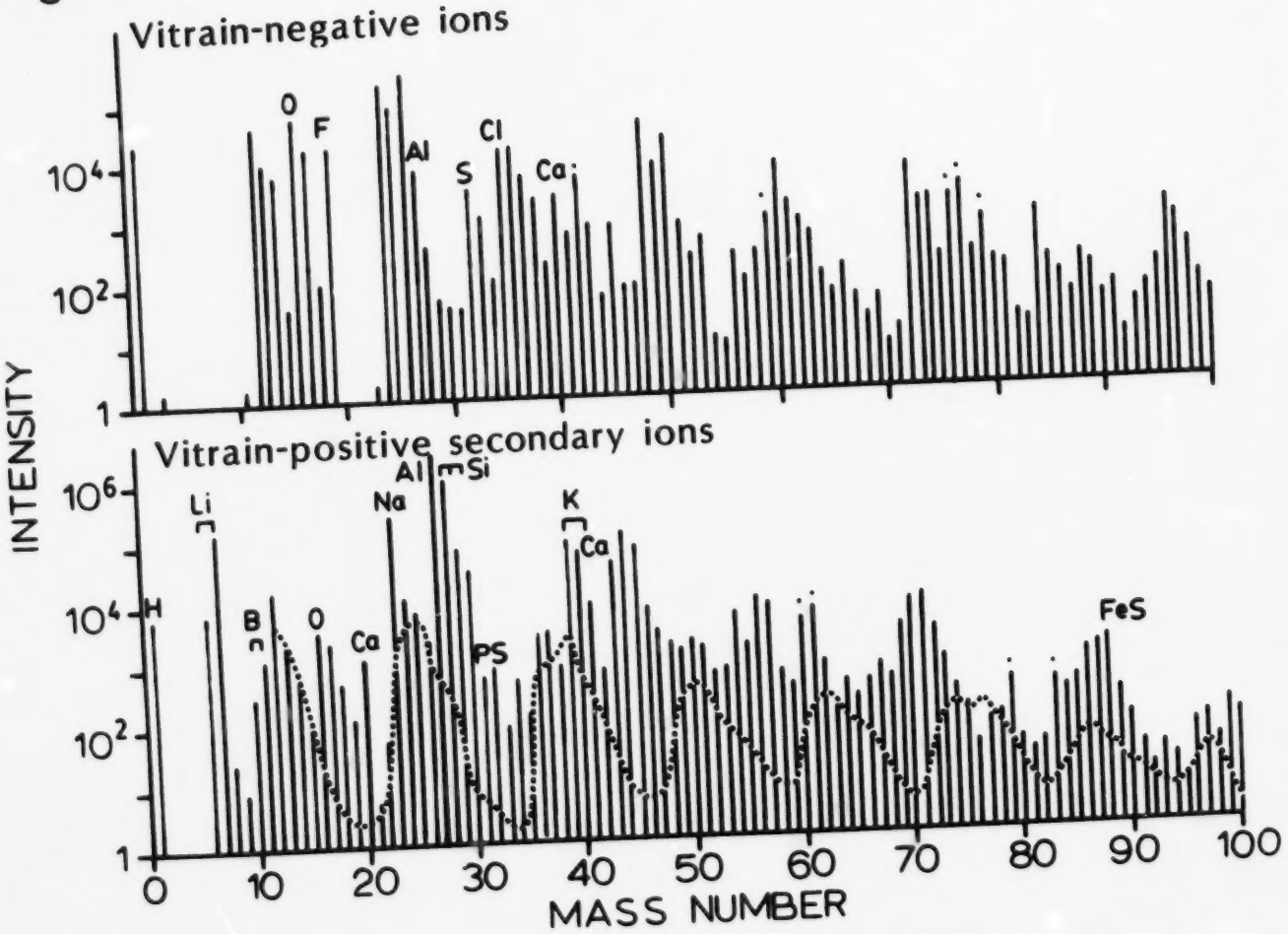
Vitrain-negative ions
O
F
Al
S
Cl
Ca
10^4
10^2
1
Vitrain-positive secondary ions
Li
Al
Si
Na
K
Ca
H
B
O
Ca
PS
FeS
10^6
10^4
10^2
1
INTENSITY
0
10
20
30
40
50
60
70
80
90
100
MASS NUMBER

Figure 6

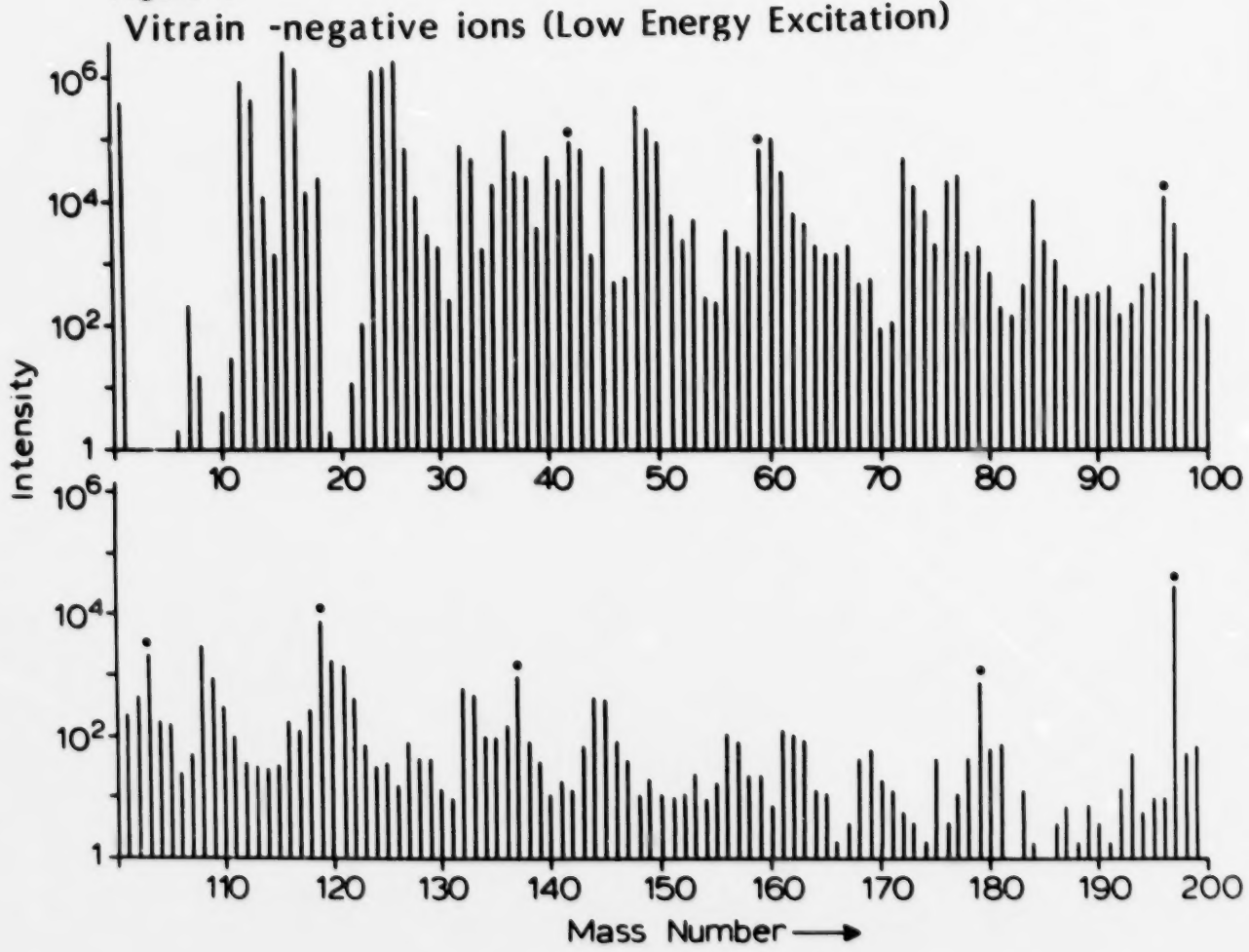
Vitrain -negative ions (Low Energy Excitation)
Intensity
10^6
10^4
10^2
1
10
20
30
40
50
60
70
80
90
100
110
120
130
140
150
160
170
180
190
200
Mass Number

Figure 7

SEM IMAGE OF SIMS LINE SCAN AREA

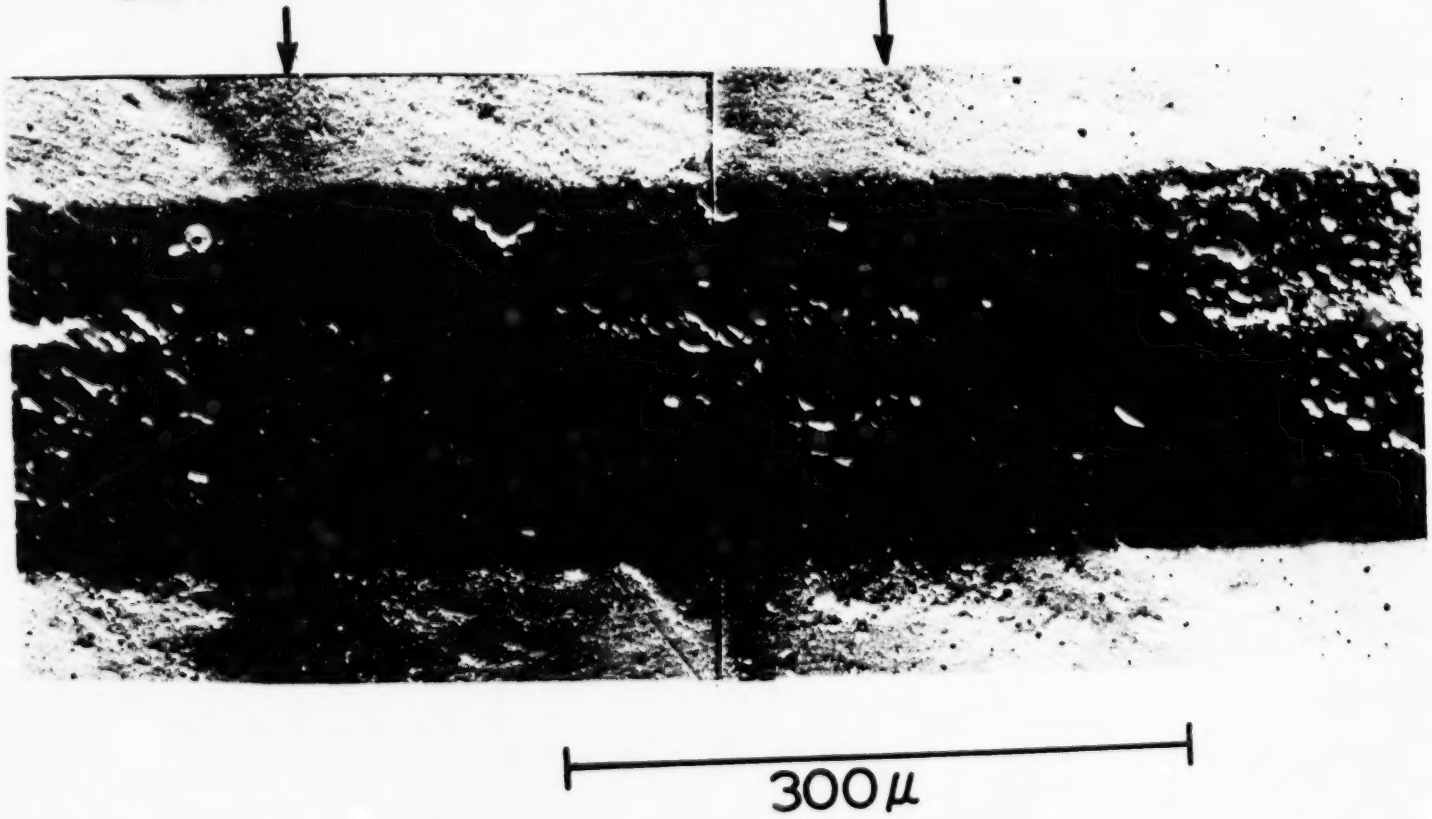

Figure 8 - Ion Intensity Line Scan Across a Coal Surface

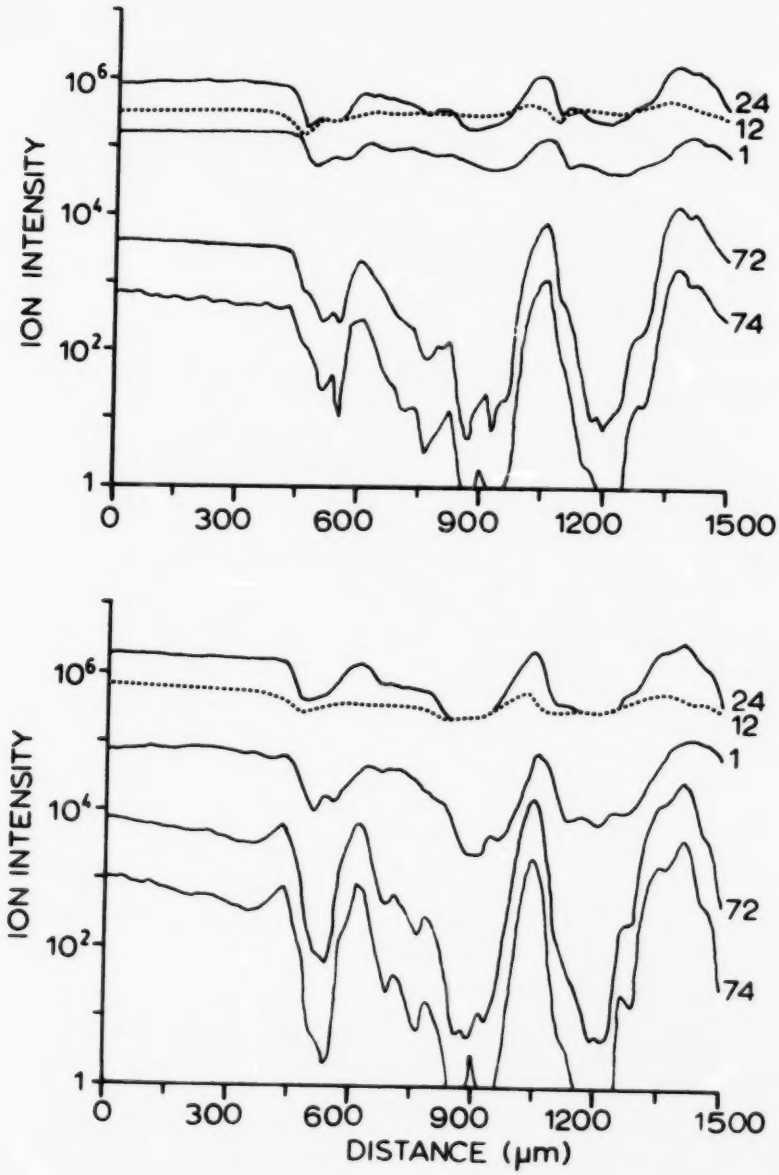

Figure 9 - Ion Images of One Area of a Vitrain Maceral (Area 1)

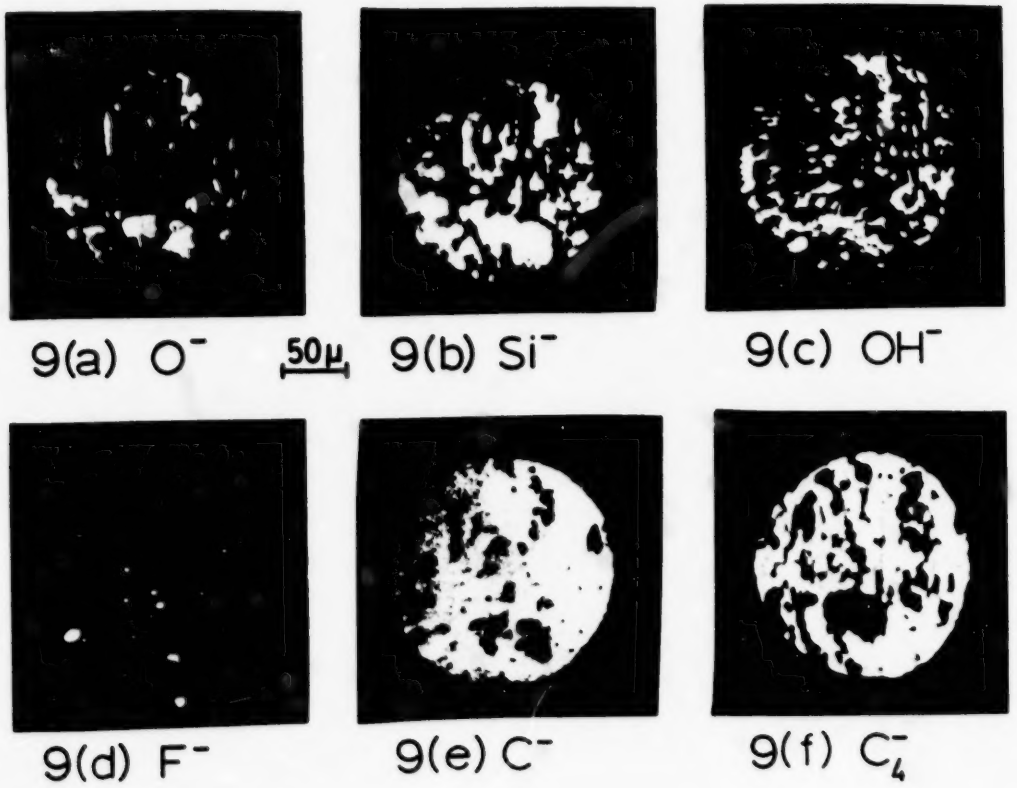

Figure 10 - Optical Micrograph of a Polished Section of the Vitrain Section Submitted

Figure 11 - Negative Ion Images of a Vitrain Surface Area 2 (150 μm field)

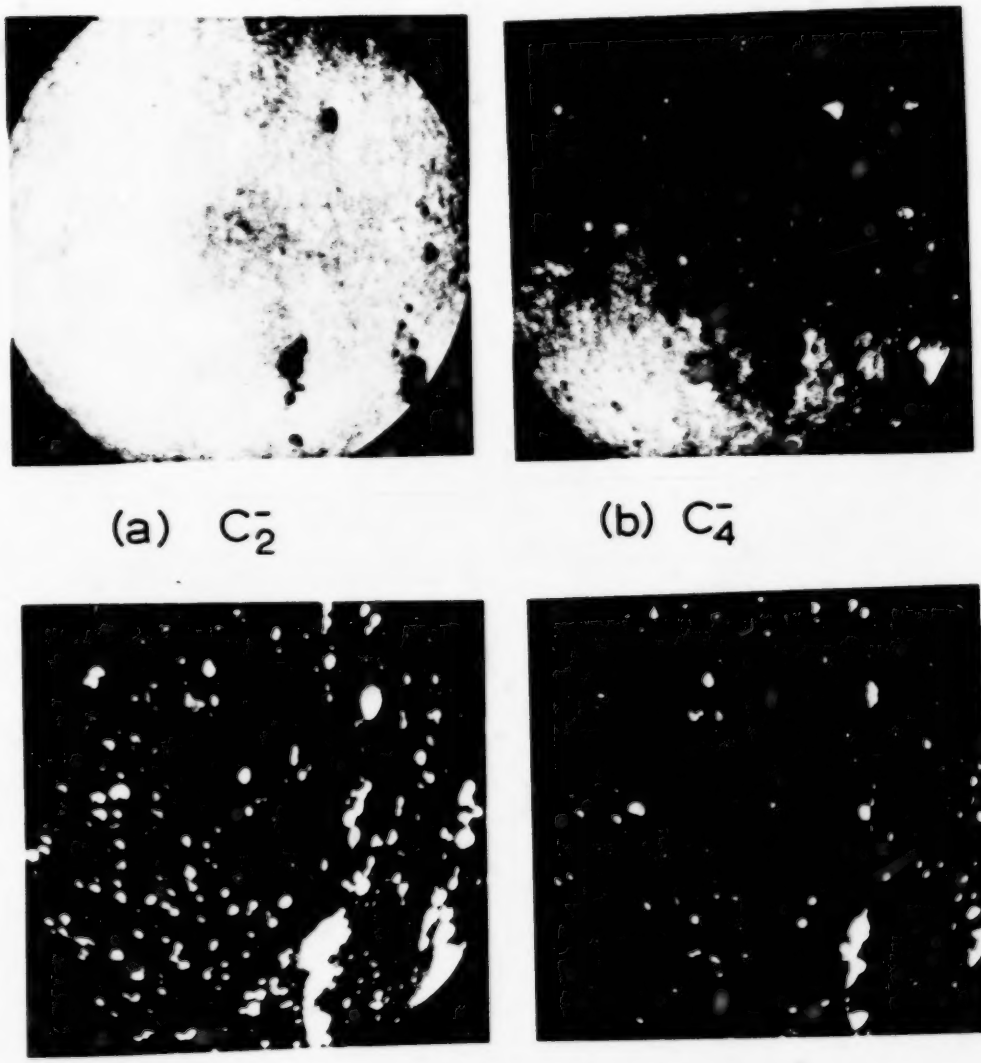

(a) C_2^- (b) C_4^-

(c) O^- (d) OH^-

Figure 12 - Ion Images of Vitrain - Area 3

12(a) O^-

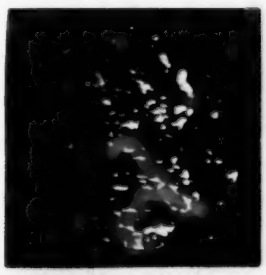

100μ 12(b) Li^+

12(c) Ti^+

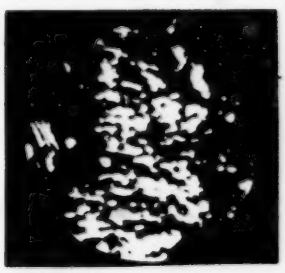

12(d) H^+

12(e) C^-

12(f) C_2^-

12(g) $C_2H_2^-$

12(h) H^-

Figure 13 Line Scans Across a Vitrain Maceral Containing Varying Oxygen Concentrations

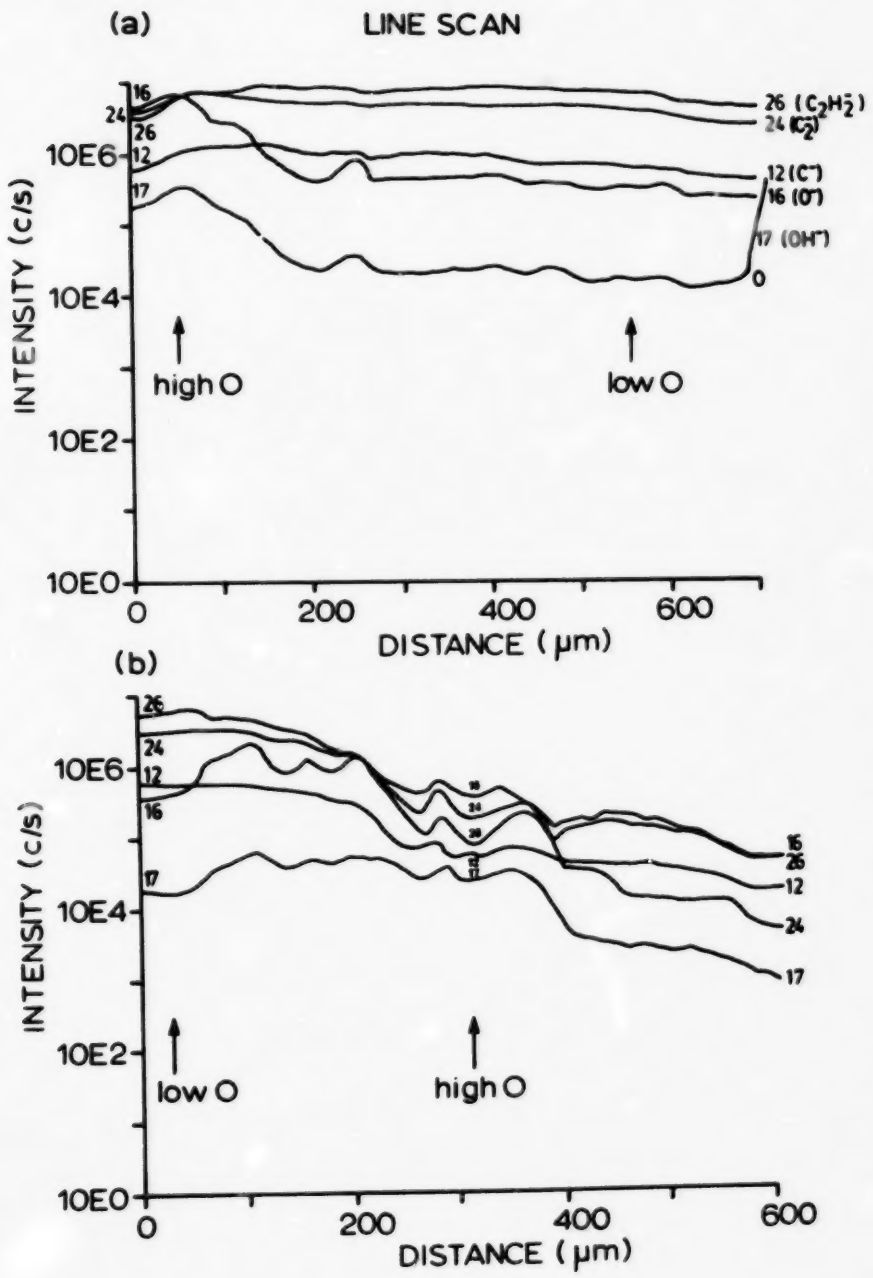

Figure 14 - Ion Images of Vitrain - Area 4

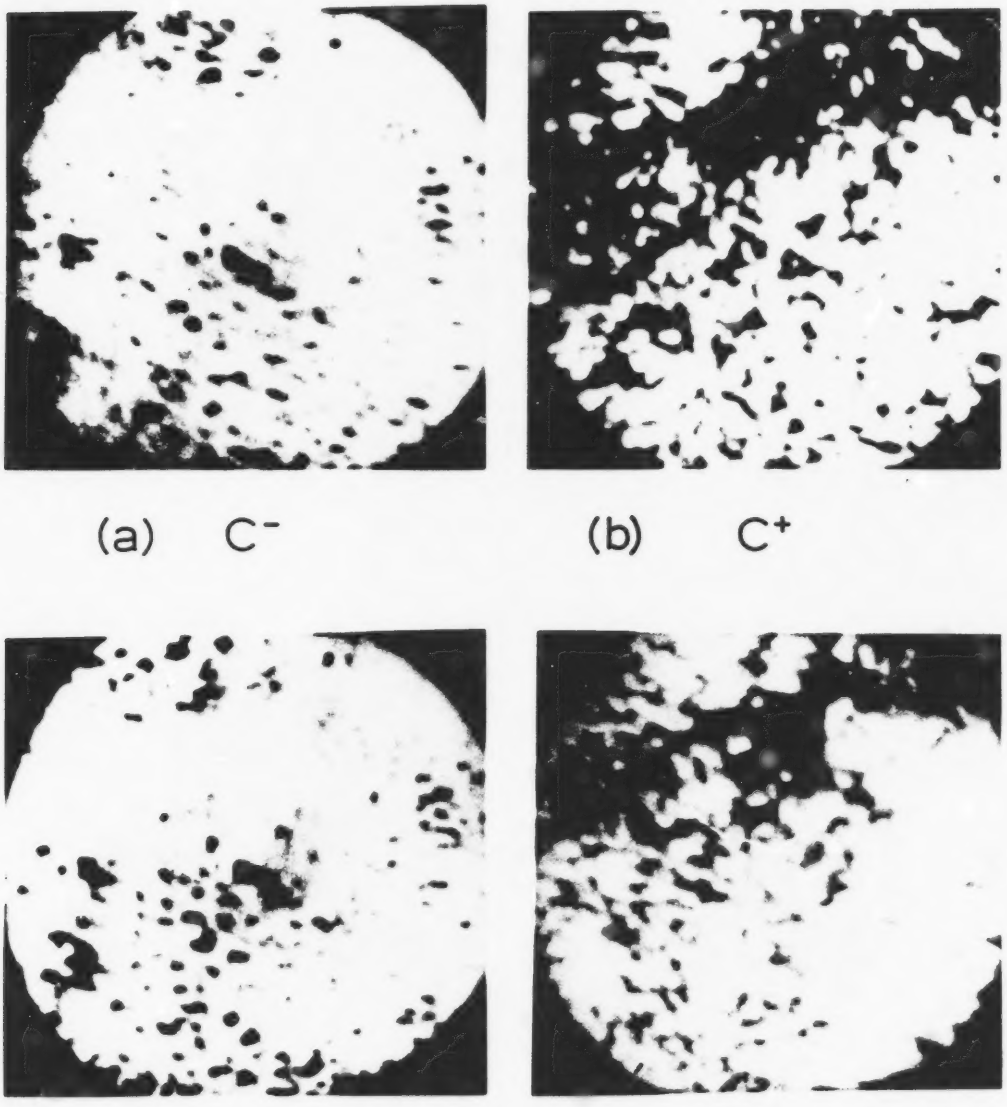

(a) C^- (b) C^+

(c) C_2^- (d) O^-

Figure 15- Scanning Electron Micrograph of Fusinite Maceral afer Analysis by SIMS

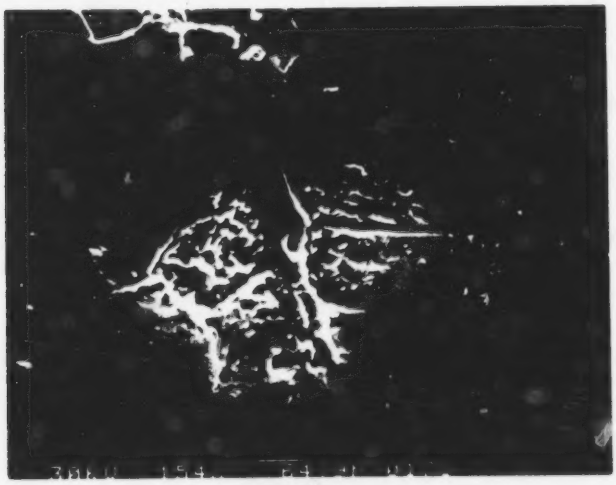

(a)

(b)

Figure 16
Negative Secondary Ion Images of a Fusinite Maceral

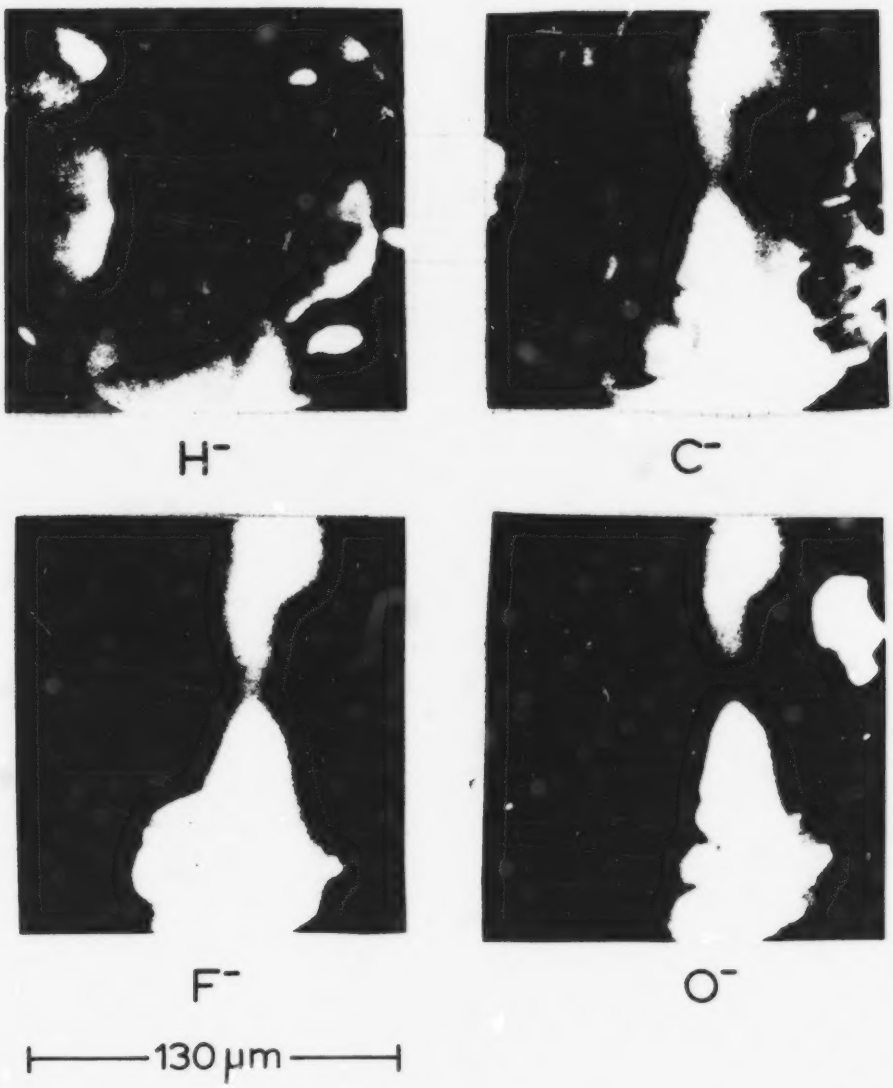

Figure 17 - Line Scan of C^-, C_2^-, $C_2H_2^-$, O^- and F^- across a small maceral of Fusinite

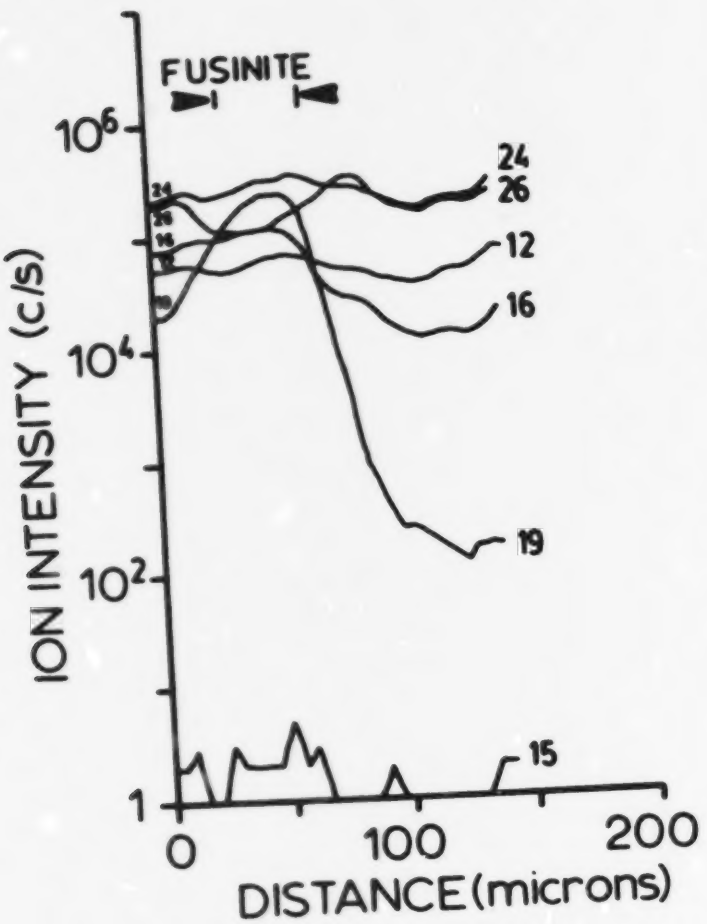

Figure 18
Positive Secondary Ion Images of a Fusinite Maceral

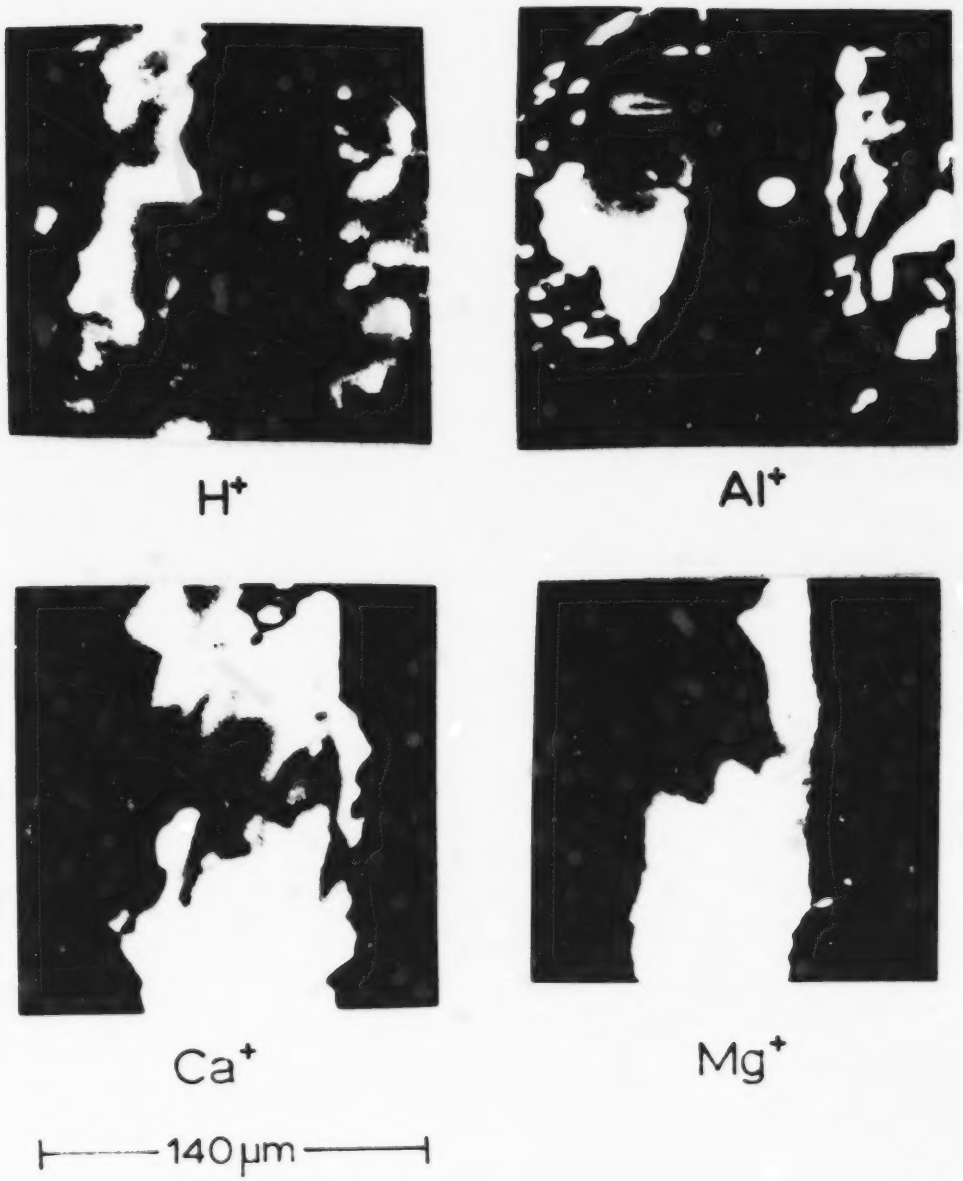

Figure 19
Negative Secondary Ion Spectrum of Fusinite

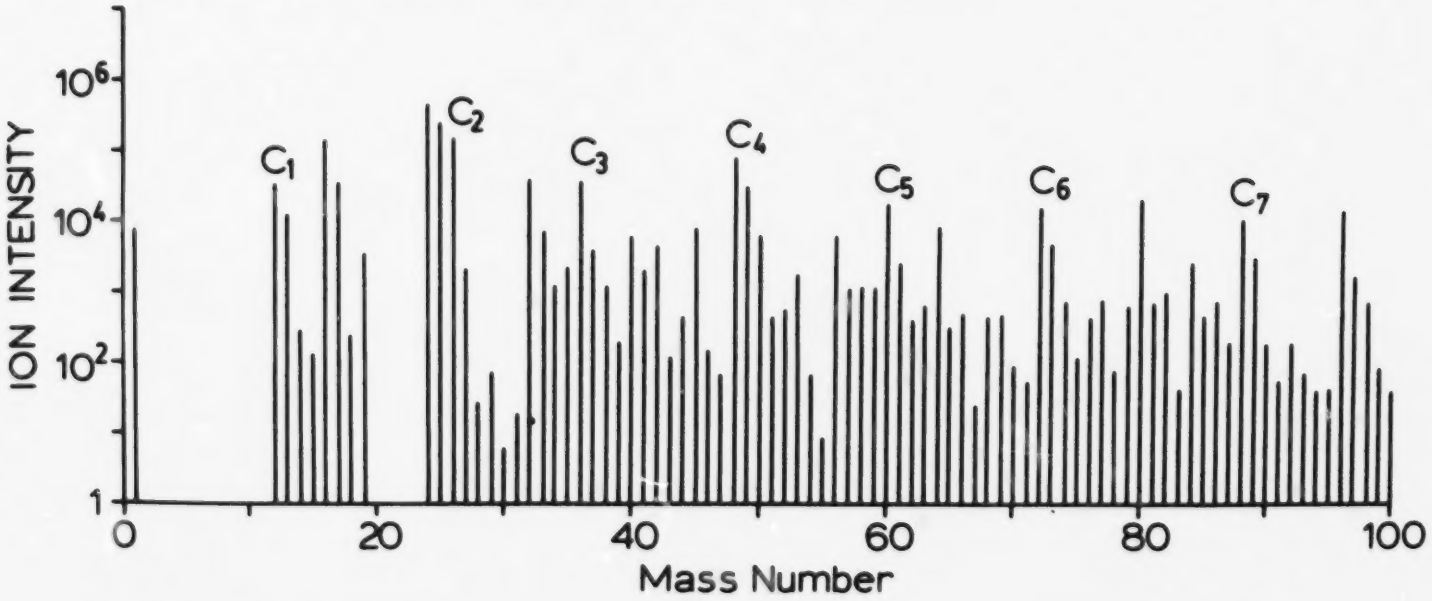

Figure 20- Ion Images of a Fusinite Maceral

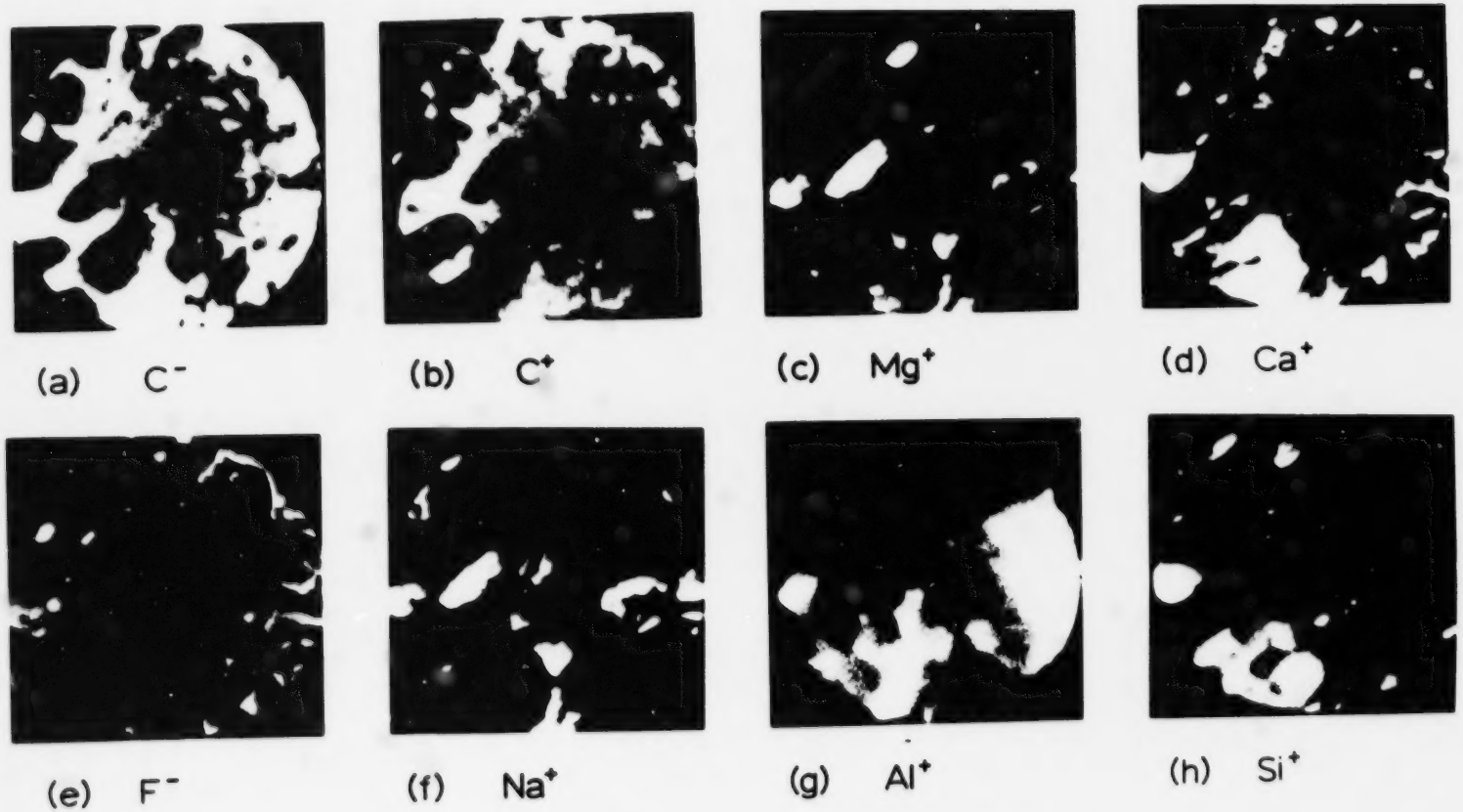

(a) C^- (b) C^+ (c) Mg^+ (d) Ca^+

(e) F^- (f) Na^+ (g) Al^+ (h) Si^+

Figure 21 - Optical Micrograph of Exinite Macerals Within a Vitrain Matrix (x100)

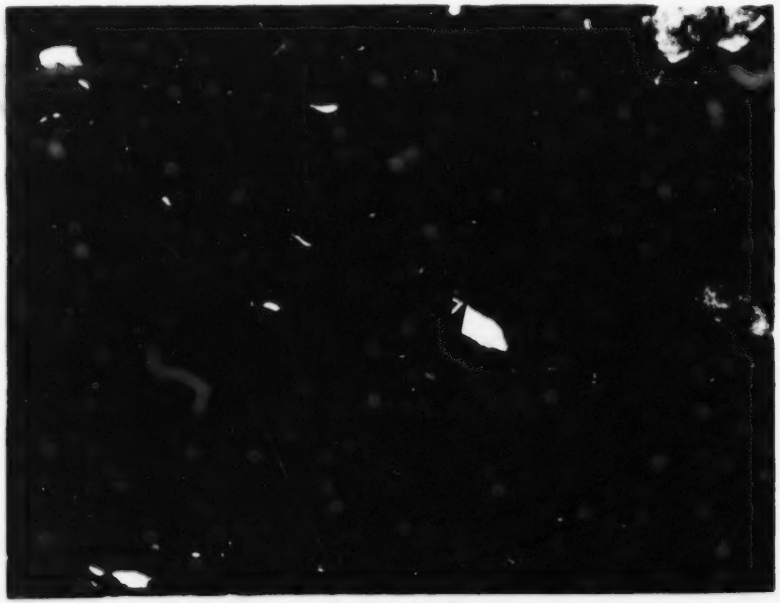

Figure 22
Secondary Ion Images of a Exinite Maceral

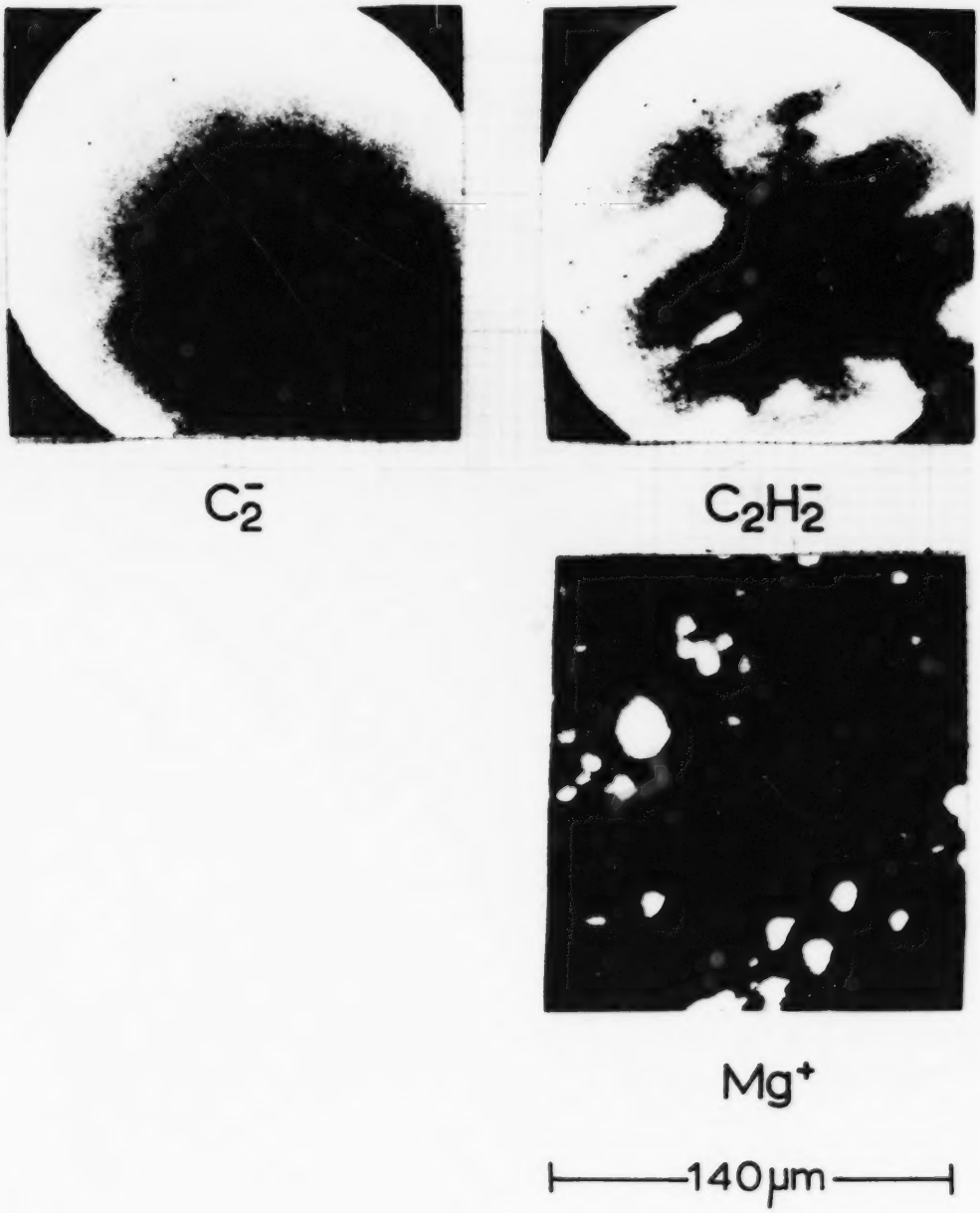

Figure 23- Ion Images of Exinite B

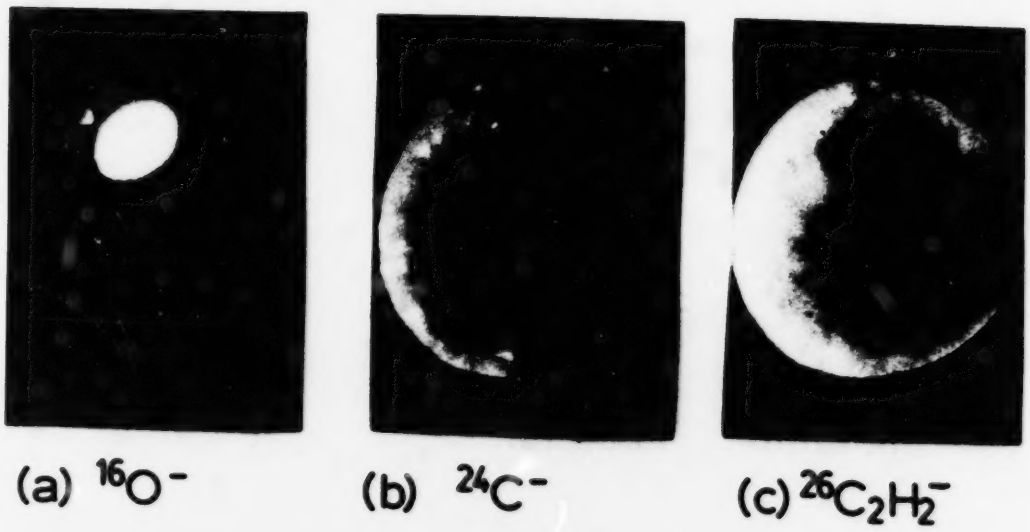

(a) $^{16}O^-$ (b) $^{24}C^-$ (c) $^{26}C_2H_2^-$

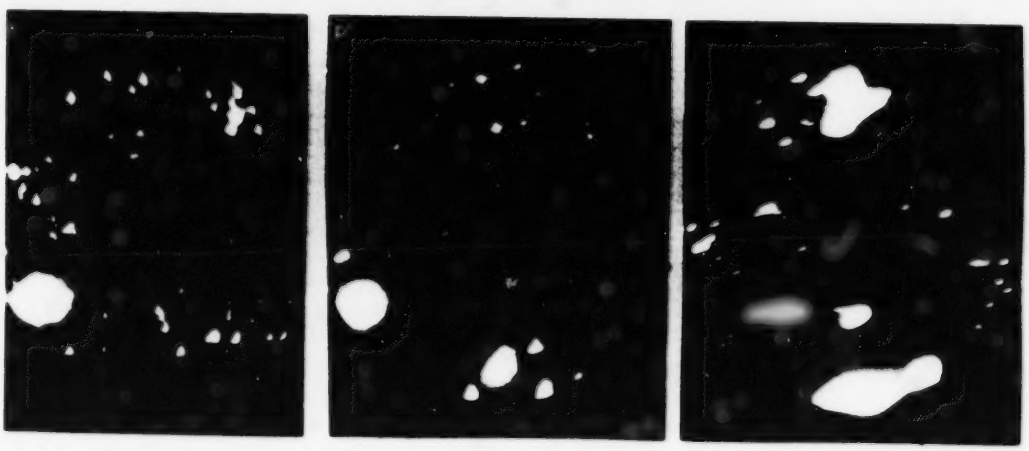

(d) $^{23}Na^+$ (e) $^{24}Mg^+$ (f) $^{56}Fe^+$

Figure 24- Optical Micrographs of Typical Areas of Specimens 251, 587 and 668

251

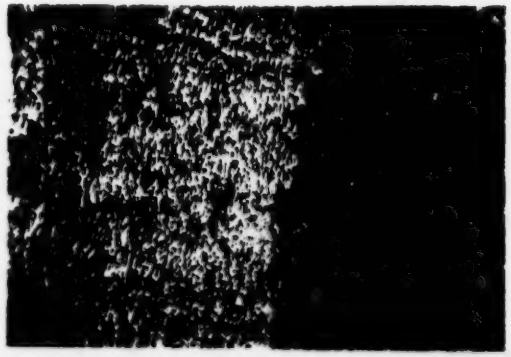

587

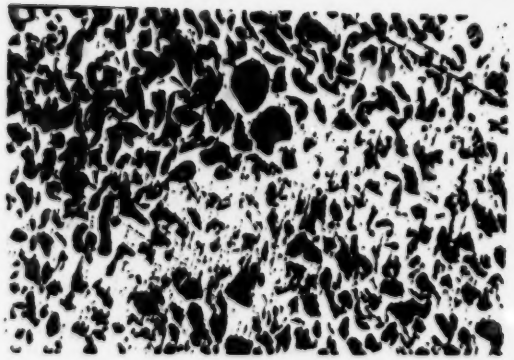

668

Figure 25 - Ion Images of P-251

(a) Ca (1sec)

(b) Al (18 sec)

(c) O^- (1sec)

(d) C^- (12 sec)

Figure 26- Ion Images of First Area of Coal P-587

(a) C^+

(b) Al^+

(d) Si^+

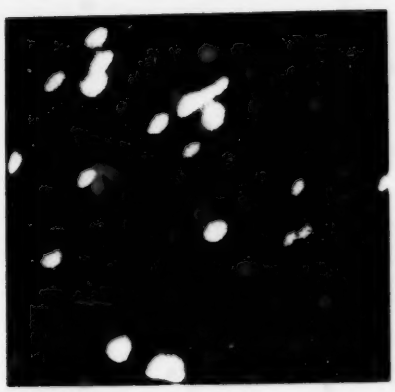

(e) Sr^+

Figure 27 - Ion Images of a Second Area of Coal P-587

(a) Ca^+

(b) Al^+

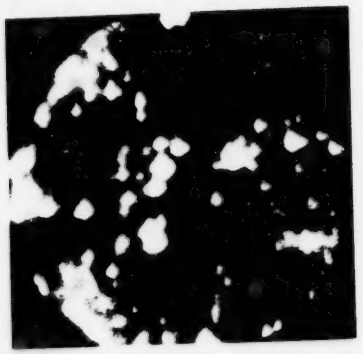

(c) Si^+

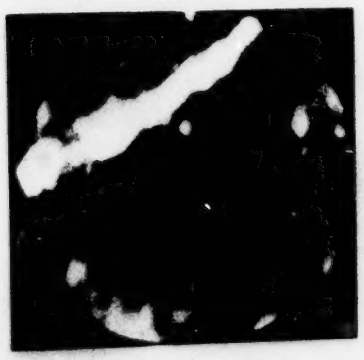

(d) Na^+

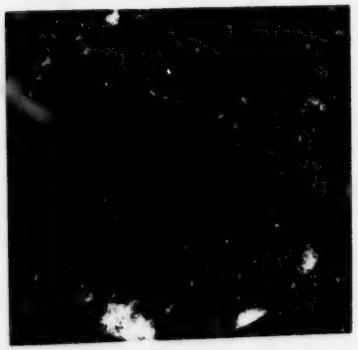

(e) B^+

Figure 28- Ion Images of Coal P-668

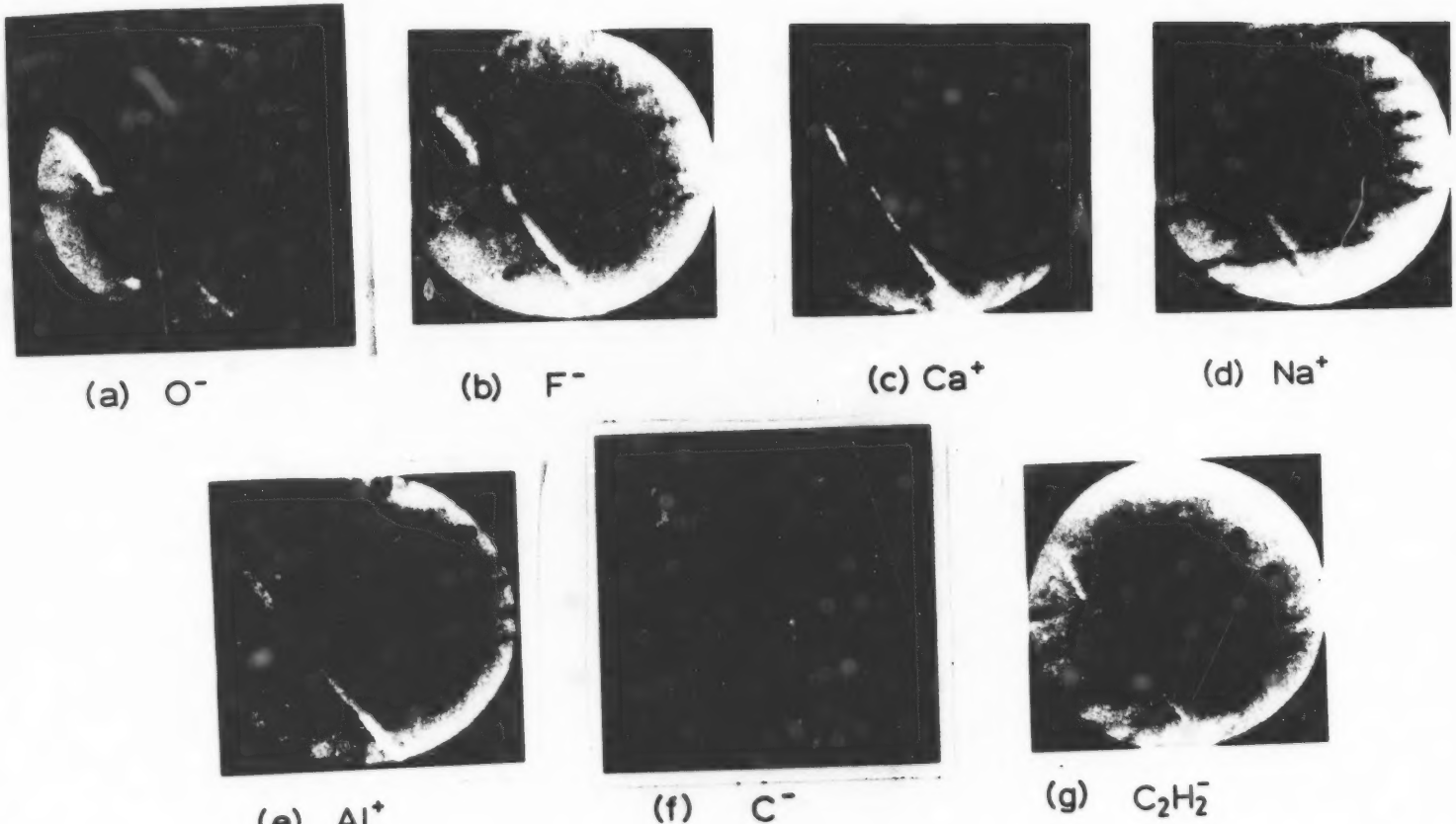

(a) O^- (b) F^- (c) Ca^+ (d) Na^+

(e) Al^+ (f) C^- (g) $C_2H_2^-$

Figure 29
Depth Profile of Oxygen and Vitrain

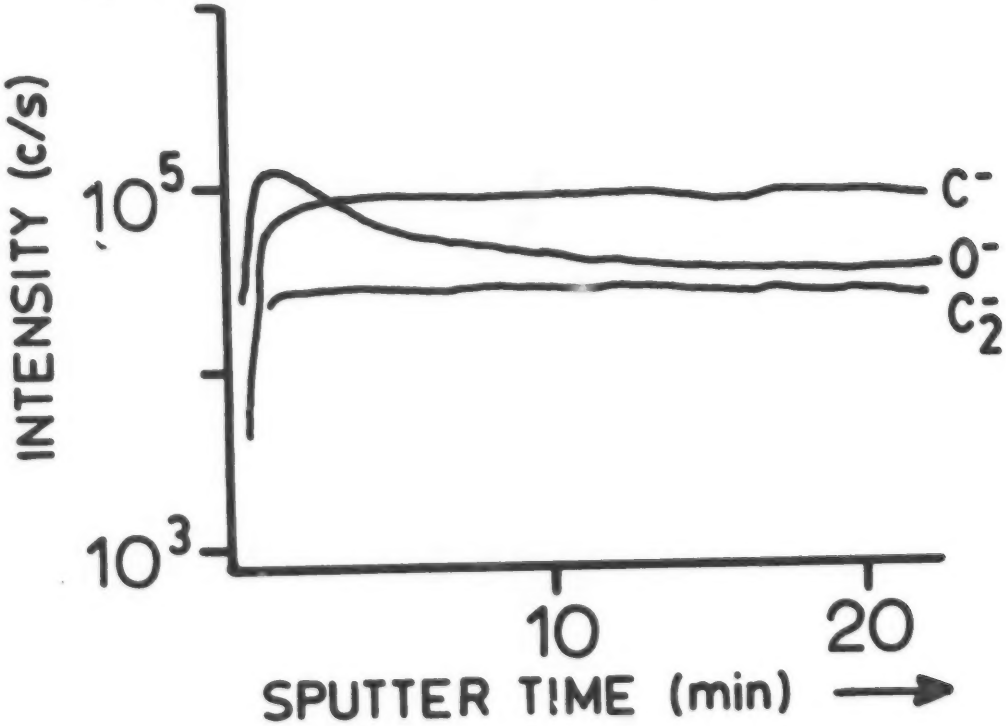

Figure 30
Oxygen-Induced Changes in Vitrain

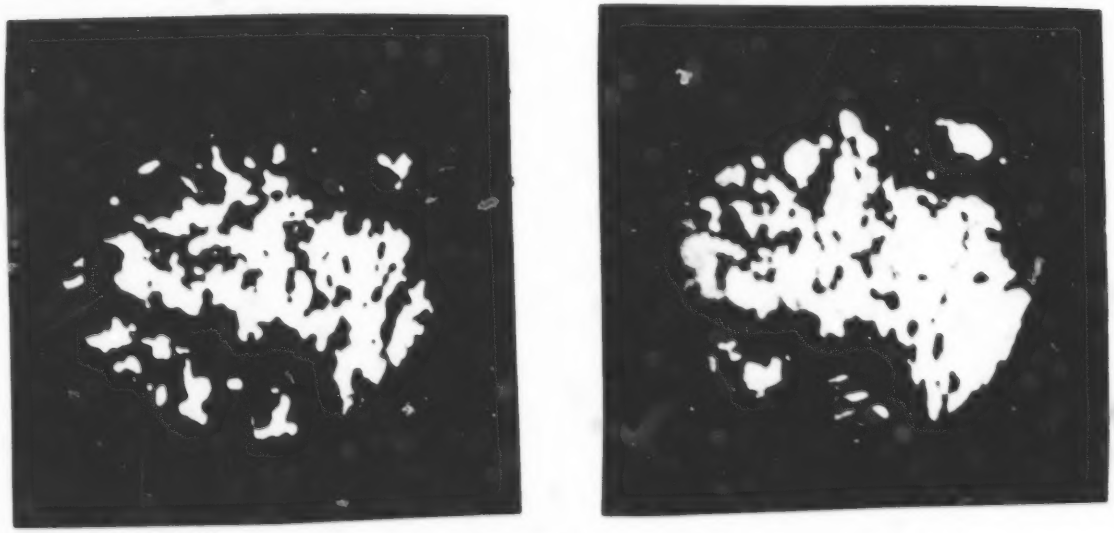

8(a) Li^+ 100μ 8(b) O^-

POOR

QUALITY

ORIGINAL